



**HAL**  
open science

## Evaluation of Sentinel-1 & 2 time series for predicting wheat and rapeseed phenological stages

Audrey Mercier, Julie Betbeder, Jacques Baudry, Vincent Le Roux, Fabien Spicher, Jérôme Lacoux, David Roger, Laurence Hubert-Moy

### ► To cite this version:

Audrey Mercier, Julie Betbeder, Jacques Baudry, Vincent Le Roux, Fabien Spicher, et al.. Evaluation of Sentinel-1 & 2 time series for predicting wheat and rapeseed phenological stages. *ISPRS Journal of Photogrammetry and Remote Sensing*, 2020, 163, pp.231-256. 10.1016/j.isprsjprs.2020.03.009 . hal-02520012

**HAL Id: hal-02520012**

**<https://hal.science/hal-02520012>**

Submitted on 22 Aug 2022

**HAL** is a multi-disciplinary open access archive for the deposit and dissemination of scientific research documents, whether they are published or not. The documents may come from teaching and research institutions in France or abroad, or from public or private research centers.

L'archive ouverte pluridisciplinaire **HAL**, est destinée au dépôt et à la diffusion de documents scientifiques de niveau recherche, publiés ou non, émanant des établissements d'enseignement et de recherche français ou étrangers, des laboratoires publics ou privés.



Distributed under a Creative Commons Attribution - NonCommercial 4.0 International License

## Evaluation of Sentinel-1 & 2 time series for predicting wheat and rapeseed phenological stages

Audrey Mercier<sup>a\*</sup>, Julie Betbeder<sup>b, c</sup>, Jacques Baudry<sup>d</sup>, Vincent Le Roux<sup>e</sup>, Fabien Spicher<sup>e</sup>, Jérôme Lacoux<sup>e</sup>, David Roger<sup>e</sup> and Laurence Hubert-Moy<sup>a</sup>

<sup>a</sup> LETG Rennes UMR 6554 LETG; Université Rennes 2, Place du recteur Henri Le Moal, Rennes Cedex 35043, France; [laurence.moy@uhb.fr](mailto:laurence.moy@uhb.fr)

<sup>b</sup> CIRAD, Forêts et Sociétés, 34398 Montpellier, France; [julie.betbeder@cirad.fr](mailto:julie.betbeder@cirad.fr)

<sup>c</sup> Ecosystems Modelling Unity, Forests, Biodiversity and Climate Change Program, Tropical Agricultural Research and Higher Education Center (CATIE), Turrialba, Cartago, Costa Rica

<sup>d</sup> INRA, UMR BAGAP, 65 rue de St-Brieuc CS 84215, Rennes Cedex 35042, France; [jacques.baudry@inra.fr](mailto:jacques.baudry@inra.fr)

<sup>e</sup> Unité Ecologie et Dynamiques des Systèmes Anthropisés, UMR 7058 CNRS, Université de Picardie Jules Verne, 33 rue St-Leu, 80039 Amiens, France; [vincent.leroux@u-picardie.fr](mailto:vincent.leroux@u-picardie.fr), [fabien.spicher@u-picardie.fr](mailto:fabien.spicher@u-picardie.fr), [jerome.lacoux@u-picardie.fr](mailto:jerome.lacoux@u-picardie.fr), [david.roger@u-picardie.fr](mailto:david.roger@u-picardie.fr)

\* Correspondence: [audrey.mercier@univ-rennes2.fr](mailto:audrey.mercier@univ-rennes2.fr); Tel.: +33-2-9914-1847

---

### Abstract

In the global context of population growth and climate change, monitoring crops is necessary to sustain agriculture and conserve natural resources. While many studies have demonstrated the ability of optical and SAR remotely sensed data to estimate crop parameters, these data have not been compared or combined to predict crop phenological stages. Despite the high sensitivity of SAR polarimetric data to crop phenological stages, no study has used high temporal resolution data. The freely available SAR Sentinel-1 (S-1) and optical Sentinel-2 (S-2) time series provide a unique opportunity to monitor crop phenology at a high spatial resolution on a weekly basis. The objective of this study was to evaluate the potential of S-1 data alone, S-2 data alone, and their combined use to predict wheat and rapeseed phenological stages. We first analyzed temporal profiles of spectral bands, vegetation indices and leaf area index (LAI) derived from S-2 data, and backscattering coefficients and polarimetric indicators derived from S-1 data. Then, an incremental procedure was used to estimate the contribution of S-1 and S-2 features to the classification of principal and secondary phenological stages of wheat and rapeseed. Results for both crops showed that the classification obtained with combined S-1 & 2 data (mean kappa = 0.53-0.82 and 0.74-0.92 for wheat and rapeseed, respectively) was more accurate than those obtained with S-2 data alone (mean kappa = 0.54-0.75 and 0.67-0.86 for wheat and rapeseed, respectively) or S-1 data alone (mean kappa = 0.48-0.61 and 0.61-0.64 for wheat and rapeseed, respectively). Combining S-1 & 2 data allowed better identification of the beginning and end of tillering for wheat and the beginning and end of ripening for rapeseed. Among S-2 features, the most important were LAI for wheat and the NDVI for rapeseed. For both crops, the S2REP index was one of the most important vegetation indices, while MCARI was less important. For S-1 features, results highlighted the large contribution of the backscatter ratio ( $\sigma^{\circ}\text{VH}:\sigma^{\circ}\text{VV}$ ) and the value of using polarimetric indicators (Shannon entropy and span) to monitor rapeseed and wheat phenology. The main novelties of this work are the use of S-1 polarimetric indicators to identify phenological stages of wheat and rapeseed and the mapping of wheat and rapeseed secondary phenological stages using remotely sensed data.

**Keywords:** Remote sensing, Multi-temporal optical and SAR data, Polarimetry, C-Band, Crop phenology

---

## 1. Introduction

Monitoring crops is important for many agricultural and ecological applications, such as estimating crop yields (Maas, 1988; Jin et al., 2018), preventing disease and insect infestation (Hatfield and Pinter, 1993), applying fertilizer (Bouchet et al., 2016; Diacono et al., 2013) and managing water resources (Duchemin et al., 2015). Identifying and predicting phenological stages provide essential information for precision agriculture. Considering specific phenological stages can optimize irrigation and fertilizer application schedules (Bouchet et al., 2016; Sakamoto et al., 2005). Some phenological stages are more sensitive to pests and diseases, thus identifying and predicting these stages can prevent pest outbreaks and diseases and reduce the use of pesticides (Vreugdenhil et al., 2018). Finally, phenological stages can be used as indicators of global warming on terrestrial ecosystems (Menzel et al., 2006). One of the main current challenges is to identify principal and secondary phenological stages of wheat and rapeseed that are two of the most important crops in the world in terms of harvested area (Food and Agriculture Organization of the United Nations, 2017). Principal phenological stages are defined as long-duration developmental phases of plants, while secondary stages are short developmental steps within them (Bleiholder, et al., 2001).

The recent Synthetic Aperture Radar (SAR) Sentinel-1 (S-1) and optical Sentinel-2 (S-2) sensors, which acquire image time-series at a high temporal frequency (every 5-12 days, depending on the acquisition mode and location in the world) and high spatial resolution (2.3 m and 13.9 m in range and azimuth directions, respectively, for S-1 bands; 10, 20 and 60 m spatial resolutions for S-2 bands), provide a unique opportunity to monitor crops regularly at fine grain scale. Moreover, S-1 & 2 data are freely available under an open license.

Several features (i.e. spectral bands, vegetation indices and biophysical variables) derived from optical remotely sensed data have demonstrated their great potential to predict crop parameters such as yield, biomass and phenological stages (Quarmby et al., 1993; Doraiswamy et al., 2004; Mulla, 2013; Bontemps et al., 2015; Pan et al., 2015; Betbeder et al., 2016). For S-2 time series, significant relationships have been found between S-2 and vegetation indices: LAI, leaf chlorophyll concentration and canopy chlorophyll content for potato crops in the Netherlands (Clevers et al., 2017) and for maize, garlic, oat, onion, potato, sunflower, alfalfa and grape crops in Spain and Italy (Frampton et al., 2013). The potential of S-2 red-edge bands for estimating LAI was demonstrated for maize, wheat, rapeseed, barley, sugar beet, sunflower, onion and other vegetable crops in Spain and Germany and for winter wheat in northern China (Pan et al., 2018). Veloso et al. (2017) found that S-2 Normalized Difference Vegetation Index (NDVI) was highly sensitive to the phenological stages of winter and summer crops in southern France. Despite these abilities, a continuous time-series of optical images is difficult – if not impossible – to acquire due to the cloud-free dependence of optical acquisitions and the signal provides information only about the top layer of vegetation. In this context, Synthetic-Aperture Radar (SAR) images are a reliable alternative to the limitations of optical images since microwaves are not sensitive to atmospheric or light conditions. Unlike optical reflectance, backscattering coefficients depend on soil conditions (roughness and moisture) during early plant phenological stages (McNairn and Brisco, 2004; Baup et al., 2007; Álvarez-Mozos et al., 2009) and later on crop properties (biomass, architecture, height) (Baghdadi et al., 2009; Fieuzal et al., 2013; Wiseman et al., 2014).

Many studies have demonstrated the relevance of airborne and spatial SAR data for identifying phenological stages (Steele-Dunne et al., 2017). In recent years, several studies have shown the value of S-1 data for

monitoring crop phenology. Bargiel (2017) improved crop classification in northern Germany using phenological stages based on S-1 time series. Vreugdenhil et al. (2018) demonstrated the high sensitivity of S-1 backscattering coefficients and the ratio of VH:VV polarizations in detecting changes in vegetation structure for rapeseed, maize and winter cereals. S-1 VV and VH polarizations have shown great potential for identifying phenological stages of wheat (Song and Wang, 2019) and rice (Mandal et al., 2018) based on analyzing temporal behavior of backscattering coefficients, but phenological stages were not classified in these studies. Studies using polarimetric features derived from RADARSAT-2 or TerraSAR-X satellite images to identify crop parameters showed that polarimetric indicators were highly sensitive to phenological stages (McNairn et al., 2018; Pacheco et al., 2016), crop height (Betbeder et al., 2016; Canisius et al., 2018), crop biomass (Wiseman et al., 2014; Jin et al., 2015; Betbeder et al., 2016; Homayouni et al., 2019) and LAI (Jiao et al., 2009; Jin et al., 2015; Betbeder et al., 2016; Canisius et al., 2018). To our knowledge, polarimetric indicators derived from S-1 data have not been used to study crop parameters.

A few studies used both optical and radar data to monitor crop phenology. Most used optical data as a reference and predicted biophysical parameters from SAR data. Betbeder et al. (2016) revealed the high potential of RADARSAT-2 polarimetry using NDVI derived from Formosat-2, SPOT-4 and SPOT-5 as references. El Hajj et al. (2019) described the ability of the S-1 C-band to penetrate crops when biomass is high ( $NDVI > 0.7$ ) for maize, and the lack of this ability for wheat and grassland. Veloso et al. (2017) showed the value of S-1 data for monitoring crop growth through analysis of temporal profiles of VV and VH polarizations and the VH:VV ratio for winter and summer crops in southern France. Although these studies highlighted the value of SAR data, they did not evaluate the potential of combining SAR and optical data to predict crop parameters. Stendardi et al. (2019) concluded that combining SAR S-1 and optical S-2 data shows promise for detecting the phenology of mountain meadows in northern Italy. Jin et al. (2015) studied the potential of vegetation indices derived from the Huanjing-1A/B optical satellite and polarimetric indicators derived from RADARSAT-2 to estimate the LAI and biomass of winter wheat. They found the highest correlations when optical and radar data were combined. While these studies evaluated SAR and optical time-series and their combined use to estimate LAI and biomass, to our knowledge, no study has explored the value of SAR S-1 and optical S-2 data for predicting phenological stages.

The objective of this study was to assess the potential of S-1 data alone, S-2 data alone, and their combined use to identify principal and secondary phenological stages of wheat and rapeseed. More specifically, this study aimed to evaluate the value of polarimetric indicators to discriminate wheat and rapeseed phenological stages and determine the number of relevant S-1 & 2 features that are needed to discriminate principal and secondary phenological stages of these crops. We evaluated the performance of spectral bands and vegetation indices derived from S-2 time-series and backscattering coefficients and polarimetric indicators derived from S-1 time-series. We first analyzed temporal profiles of features derived from S-1 and S-2 time-series for wheat and rapeseed crops. Satellite images were then classified using an incremental procedure based on the importance rank of these input features (Mercier et al., 2019). This method automatically selects important features to classify the phenological stages of wheat and rapeseed.

The novelties of this work are threefold: (i) The use of S-1 polarimetric indicators to identify principal and secondary phenological stages of wheat and rapeseed; (ii) The statistical analysis of optical data, SAR data and their combined use to discriminate phenological stages of wheat and rapeseed; (iii) Mapping of wheat and rapeseed secondary phenological stages using remotely sensed data.

## 2. Materials

### 2.1 Study area

The study area consisted of two  $5 \times 5$  km sub-sites in northern France (Fig. 1). Their climate is oceanic with a mean annual temperature of  $10^{\circ}\text{C}$  and mean annual precipitation of 702 mm (Météo France). The western site is located in an open field landscape with intensive cultivation of cereals and sugar beet. The eastern site is located in a “bocage” landscape dominated by grasslands and is characterized by less intensive farming activities (mainly dairy cattle) and smaller fields that tend to be enclosed by hedgerows. Both landscapes contain managed forest fragments that are used mainly for hunting and production of wood (Jamoneau, 2010)). The topography of the study area is quite flat, elevation of the “bocage” and open field landscapes ranging from 125 to 224 m (mean = 180 m) and 72 to 158 m (mean = 114 m), respectively. The geological substrate is composed of chalk in the open field landscape and silt in the “bocage” landscape (Jamoneau, 2010).

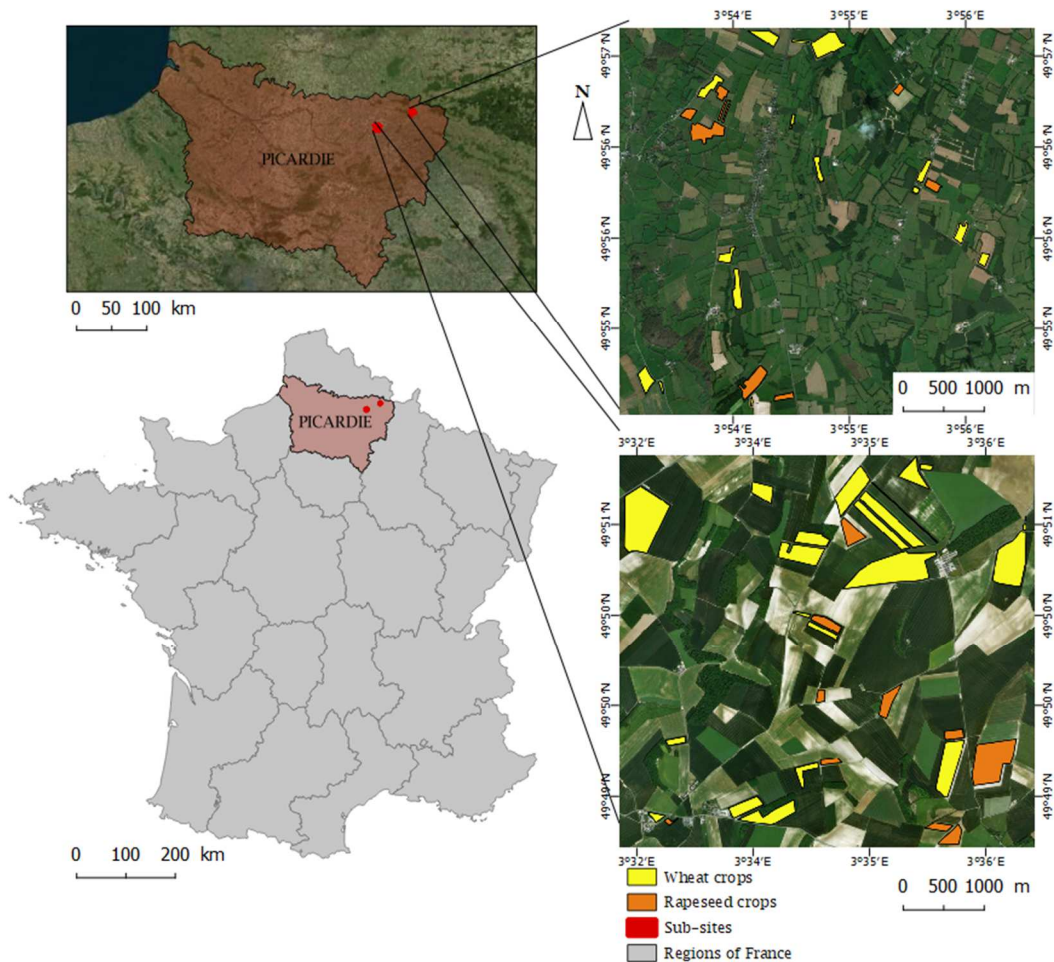


**Figure 1.** Location of the two sub-sites of the study area (bocage at the top, open field at the bottom) and the sampled fields (Sources: © EuroGeographics for the administrative boundaries; Bing © 2019, Microsoft Corporation © 2019, and DigitalGlobe © CNES 2019 Distribution Airbus DS for aerial photographs).

## 2.2 Satellite imagery

A series of five optical S-2 and eight SAR S-1 images were downloaded from January to July 2017 to cover crop cycles of wheat and rapeseed (Fig. 2). The S-1 images were acquired in Interferometric Wide (IW) swath mode and delivered with VV and VH polarizations. We used the Single Look Complex (SLC) product, which consists of focused SAR data that use the full C-signal bandwidth and preserve the phase information, to derive polarimetric indicators. The incidence angle of images ranged from 30.6-46.0° (Table 1). The ground spatial resolution was 2.5 m and the azimuth spatial resolution was 13.9 m (Table 1). According to data recorded at the Météo-France weather station in Saint Quentin (49°49'06"N, 3°12'22"E, located 24 km from the open field site and 52 km from the "bocage" site), two S-1 images (DOY 69 and 182) were acquired after a rainfall event. The weather station recorded a rainfall of 2.6 mm and 10.1 mm on days 68 and 182, respectively. However, the radar signal was not affected by rainfall or freezing on acquisition dates, no peak being observed in the temporal profiles of VH and VV polarizations (Fig. 2).

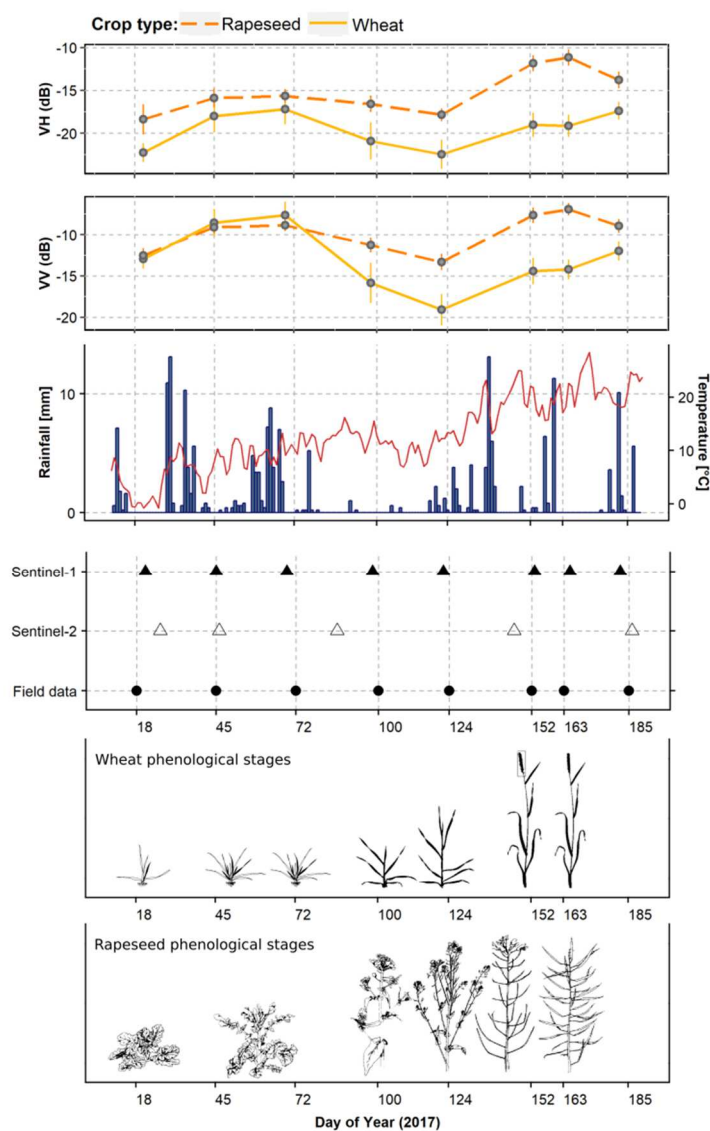


**Figure 2.** Days of year of satellite images (triangular shape), field surveys (circular shape) and main crop phenological stages for wheat and rapeseed (drawings) (Bleiholder, et al., 2001). The ombrothermal diagram (Météo France) shows climatic conditions on the image acquisition dates and temporal profiles show the mean

and standard deviation of the Sentinel-1 backscattering coefficients for wheat and rapeseed. The radar signal was not affected by rainfall (blue columns) or freezing (red lines) on acquisition dates.

**Table 1.** Main characteristics of Sentinel-1 SLC images.

Band	C (center frequency of 5 405 GHz)
Mode	Interferometric Wide Swath
Product type	Single Look Complex
Ground Resolution	2.3 m
Azimuth resolution	13.9 m
Temporal resolution	6 days
Orbit	Ascending
Polarization	Dual (VV & VH)
Swath	250 km
Incidence angle	30.6-46.0°

The S-2 images were acquired with spatial resolutions of 10 and 20 m, and a spectral resolution of 10 bands (Table 2). The tiles were downloaded in level 2A, which provides Top of Canopy reflectance and a cloud and shadow mask (ESA, 2019b). Only two S-2 images were acquired between DOY 72 and 163 due to heavy cloud cover during the spring.

**Table 2.** Main characteristics of Sentinel-2 MSI L2A images.

Spatial and spectral resolutions	10 × 10 m
	B2 (490 nm), B3 (560 nm), B4 (665 nm) and B8 (842 nm)
Temporal resolution	20 × 20 m
	B5 (705 nm), B6 (740 nm), B7 (783 nm), B8a (865 nm), B11 (1610 nm), B12 (2190 nm)
Swath	5 days
	290 km

### 2.3 Field data collection

Field surveys were conducted on 36 and 19 fields of wheat (*Triticum aestivum L.*) and rapeseed (*Brassica napus L.*), respectively (Fig. 1). Sizes of wheat and rapeseed fields ranged from 0.77-35.09 ha (mean=7.31 ha), median=4.63) and 1.35-23.91 ha (mean=4.82 ha, median=2.84 ha), respectively. Phenological stages were identified on 8 dates from January to July 2017 (Fig. 2) based on the Biologische Bundesanstalt, Bundessortenamt and Chemical industry (BBCH) scale (Bleiholder, et al., 2001). Five principal phenological stages were observed for both crops, and 29 and 15 secondary phenological stages were identified for wheat (Table 3) and rapeseed (Table 4), respectively. The samples of secondary phenological stages available for wheat and rapeseed were grouped into sub-classes to obtain a sufficient number of samples per class to train and validate the classifications.

**Table 3.** Phenological stages of wheat considered in this study and number of field observations for each secondary stage

Principal stage	Sub-class	2° stage	Description	Number of observations
Tillering	1	20	No tillers	1
		21	Beginning of tillering: first tiller detectable	14
		22	2 tillers detectable	16
		23	3 tillers detectable	18
	2	24	4 tillers detectable	22
		25	5 tillers detectable	6
		26	6 tillers detectable	8
		29	9 tillers detectable	20
		Stem elongation	3	30
31	First node at least 1 cm above tillering node			25
32	Node 2 at least 2 cm above node 1			6
33	Node 3 at least 2 cm above node 2			24
34	Node 4 at least 2 cm above node 3			9
Flowering, anthesis	4	35	Node 5 at least 2 cm above node 4	3
		65	Full flowering: 50% of anthers mature	3
		66	Full flowering: 60% of anthers mature	2
		67	Full flowering: 70% of anthers mature	3
		68	Full flowering: 80% of anthers mature	4
Development of fruit	5	69	End of flowering	9
		71	Watery ripe: first grains have reached half their final size	14
		72	Watery ripe / Early milk	2
		73	Early milk (the content of the kernel is milky)	13
		75	Medium milk: grain content milky, grains reached final size, still green	19
Ripening	6	77	Late milk	4
		83	Early dough (the content of the kernel is doughy)	10
		84	Early dough/ Soft dough ((the content of the kernel is doughy)	5
	7	85	Soft dough: grain content soft but dry. Fingernail impression not held	3
		87	Hard dough: grain content solid. Fingernail impression held	9
		89	Fully ripe: grain hard, difficult to divide with thumbnail	8

**Table 4.** Phenological stages of rapeseed considered in this study and number of field observations for each secondary stage

Principal stage	Sub-class	2° stage	Description	Number of observations
Leaf development	1	17	7 leaves unfolded	4
		18	Beginning of tillering: first tiller detectable	7
		19	2 tillers detectable	7
Inflorescence emergence	2	50	Flower buds present, still enclosed by leaves	10
		51	Flower buds visible from above ("green bud")	26
Flowering	3	60	First flowers open	1
		62	20% of flowers on main raceme open	1
		63	30% of flowers on main raceme open	5
	4	64	40% of flowers on main raceme open	5
		65	Full flowering	7
		67	Flowering declining: majority of petals fallen	7
Development of fruit	5	69	End of flowering	12
		77	70% of pods have reached their final size	1
Ripening	6	79	Nearly all pods have reached final size	12
		80	Beginning of ripening	25
	7	89	Fully ripe	19



### 3. Methods

We developed a method to analyze temporal behaviors of S-1 and S-2 features and predict phenological stages of wheat and rapeseed (Fig. 3). First, the SAR S-1 and optical S-2 signals were preprocessed and the median was computed at the field scale with a negative buffer of 15m. Second, temporal profiles were plotted based on the mean and standard deviation derived from the median for all sampled wheat and rapeseed fields. Field surveys were used to analyze the temporal profiles of the spectral bands and vegetation indices derived from S-2 and radar backscattering coefficients and polarimetric indicators derived from S-1. Finally, we assessed the potential of S-1 data alone, S-2 data alone, and combined S-1 & 2 data to predict principal and secondary phenological stages of wheat and rapeseed using an incremental method developed by Mercier et al. (2019) and field data were used as reference data to train the classifier.

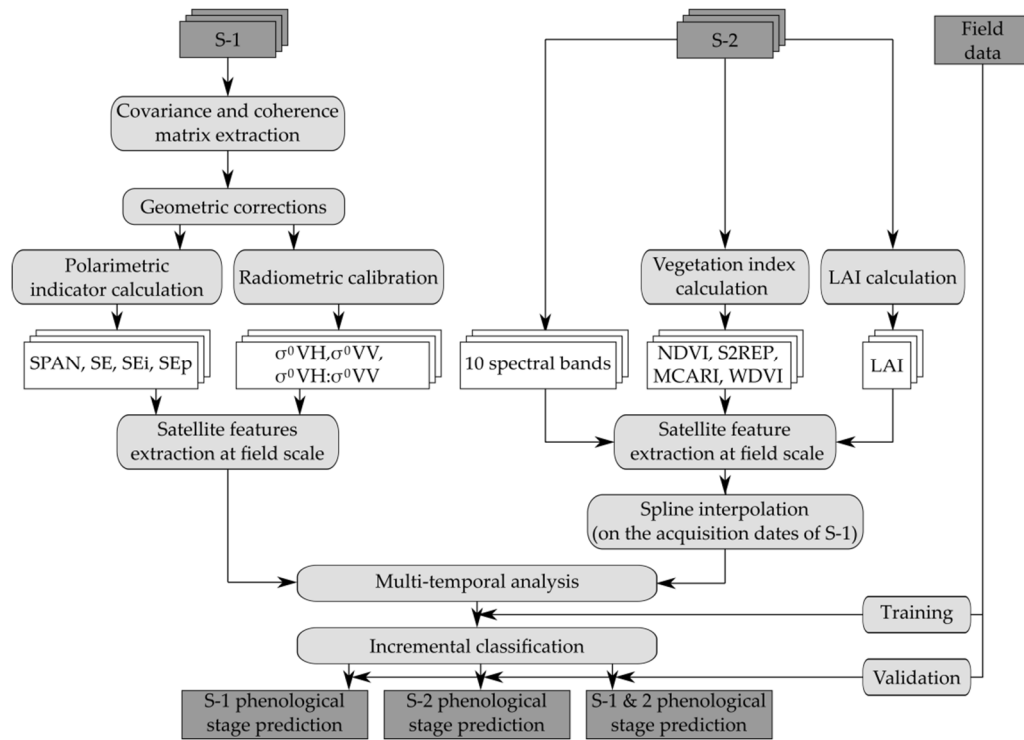


**Figure 3.** Flowchart of the image processing procedure applied to S-1 and S-2 time series to identify wheat and rapeseed secondary phenological stages.

#### 3.1 SAR Sentinel-1 image preprocessing

##### 3.1.1 Backscattering coefficients

Backscattering coefficients from S-1 images were extracted using the Sentinel-1 Toolbox (ESA, <http://step.esa.int/main/toolboxes/sentinel-1-toolbox/>). The images were first radiometrically calibrated to transform the digital number (DN, amplitude of the backscattering signal) of each pixel into backscattering coefficients ( $\sigma^0$ VV,  $\sigma^0$ VH) on a linear scale using the following equation (Miranda and Meadows, 2015):

$$value(i) = \frac{|DN_i|}{A_i^2} \quad (1)$$

where A is the information necessary to convert SAR reflectivity into physical units provided in the Calibration Annotation Data Set in the image metadata.

A refined Lee filter was then applied in a window of  $7 \times 7$  pixels to reduce speckle noise (Lee et al., 1994). The images were geocoded using Shuttle Radar Topography Mission data to correct topographic deformations (geometric correction accuracy  $< 1$  pixel). A backscattering ratio was calculated by dividing  $\sigma^{\circ}VH$  by  $\sigma^{\circ}VV$ . All images were then converted from linear to decibel (dB) scale using the following equation:

$$\sigma^0(db) = 10 \times \log_{10}(\sigma^0) \quad (2)$$

### 3.1.2 Polarimetric indicators

A  $2 \times 2$  covariance matrix ( $C_2$ ) was first extracted from the scattering matrix S of each SLR image using PolSARpro version 5.1.3 software (Pottier and Ferro-Famil, 2012). A refined Lee filter was then applied in a window of  $7 \times 7$  pixels to reduce speckle noise (Lee et al., 1994). Then, we calculated the total scattered power called span in the case of a polarimetric radar system (Ferro-Famil and Pottier, 2014). Shannon Entropy (SE), which measures the randomness of scattering of a pixel (e.g. due to variation in backscattering power or polarization), was calculated from the covariance matrix ( $C_2$ ) using the following equation:

$$SE = \log(\pi^2 e^2 |C_2|) = SE_i + SE_p \quad (3)$$

where  $SE_i$  is related to the intensity and  $SE_p$  to the degree of polarization.

Finally,  $SE$ ,  $SE_i$  and  $SE_p$  were normalized as  $SE \text{ norm}$ ,  $SE_i \text{ norm}$  and  $SE_p \text{ norm}$  using PolSARpro version 5.1.3 software.

## 3.2 Optical Sentinel-2 image preprocessing

Twelve vegetation indices were calculated since their potential to monitor crop parameters (LAI, chlorophyll content and phenological stages) using S-2 data has been demonstrated (Daughtry et al., 2000; Frampton et al., 2013; Herrmann et al., 2011; Clevers and Gitelson, 2013; Clevers et al., 2017). We calculated NDVI, the Green Normalized Vegetation Index (GNDVI), the Red-Edge Inflation Point (REIP) index, the Inverted Red-Edge Chlorophyll Index (IRECI), the Sentinel-2 Red-Edge Position (S2REP) index, the Modified Chlorophyll Absorption in Reflectance Index (MCARI), the MERIS Terrestrial Chlorophyll Index (MTCI), the Soil-Adjusted Vegetation Index (SAVI), the Modified Soil-Adjusted Vegetation Index (MSAVI), the Weighted Difference Vegetation Index (WDVI), the Pigment Specific Simple Ratio (PSSRa) and the Normalized Difference Index (NDI). Based on analysis of their temporal profiles and on correlation matrices (Appendix A), we ultimately selected four of these indices: NDVI, S2REP, MCARI and WDVI (Table 5). First, we selected NDVI because it is a very commonly used vegetation index sensitive to chlorophyll content, calculated from bands 4 and 7 of S-2 (Hermann et al., 2011; Frampton et al., 2013). Second, we chose the S2REP because this index is a version of the REP estimate for S-2 derived from a linear interpolation that incorporates bands 5 and 6 positioned on the red-edge slope (Guyot and Baret, 1988; Clevers et al., 2002). MCARI and WDVI were also selected, because they had the lowest correlations with the other features derived from S-2 for both crop types. The MCARI, which was developed to study variations in chlorophyll and minimize effects of non-photosynthetic materials,

was derived from bands 3, 4 and 5 of S-2 (Daughtry et al., 2000). The WDV, which is related to the chlorophyll content of the canopy was used to estimate LAI to avoid destructive measurements. It is a two-dimensional greenness index derived from bands 4 and 8 of S-2 (Bouman et al., 1992).

**Table 5.** Vegetation indices calculated from Sentinel-2 images. G = Green, R = Red, RE = Red-Edge, NIR = Near-infrared, NDVI = Normalized Vegetation Index, S2REP = S-2 Red-Edge Position index, MCARI = Modified Chlorophyll Absorption in Reflectance Index, WDV = Weighted Difference Vegetation Index.

Index	Equation	S-2 bands used	Original author
NDVI	$(\text{NIR}-\text{R})/(\text{NIR}+\text{R})$	$(\text{B7}-\text{B4})/(\text{B7}+\text{B4})$	(Rouse et al., 1973)
S2REP	$705 + 35 - (((\text{NIR} + \text{R})/2) - \text{RE1})/(\text{RE2} - \text{RE1})$	$705 + 35 * (((\text{B7} + \text{B4})/2) - \text{B5})/(\text{B6} - \text{B5})$	(Guyot and Baret, 1988)
MCARI	$[(\text{RE} - \text{R}) - 0.2(\text{RE} - \text{G})] * (\text{RE} - \text{R})$	$[(\text{B5} - \text{B4}) - 0.2(\text{B5} - \text{B3})] * (\text{B5} - \text{B4})$	(Daughtry et al., 2000)
WDVI	$(\text{NIR} - 0.5 * \text{R})$	$(\text{B8} - 0.5 * \text{B4})$	(Clevers, 1988)

LAI, a biophysical variable that describes the state of vegetation cover and provides information on the density of green vegetation, was also derived from S-2 images using the PROSAIL radiative transfer model implemented in SNAP v6.0 software. The spectral bands, vegetation indices and LAI were interpolated daily using a spline method to match the dates of SAR S-1 acquisition using the stats package of R software. All S-1 and S-2 images were projected onto the RGF93/Lambert-93 system (EPSG 2154) and resampled to the resolution of 10 m. In total, we preprocessed 120 S-2 features (10 spectral bands, 4 vegetation indices and 1 biophysical variable  $\times$  8 dates) and 56 S-1 features (2 backscattering coefficients, 1 backscatter ratio and 4 polarimetric indicators  $\times$  8 dates). Due to strong correlations between the S-2 spectral bands, we subsequently selected a sub-set of bands for the incremental classification based on their temporal behaviors.

### 3.3 Incremental classification

From an operational point of view, it is necessary to minimize the time between data acquisition and delivery of results to decision-makers (Hatfield et al., 2019). The time-consuming processing of multi-temporal remote sensing data is a limitation for this purpose. Therefore, we used an incremental procedure based on the importance rank of the input features to find a trade-off between accuracy and processing time (Mercier et al., 2019). This method automatically selects important features to maintain a minimum but sufficient number of features to classify the phenological stages of wheat and rapeseed. This method was applied to predict the principal and sub-classes of secondary phenological stages of wheat (Table 3) and rapeseed (Table 4) (Fig. 4).

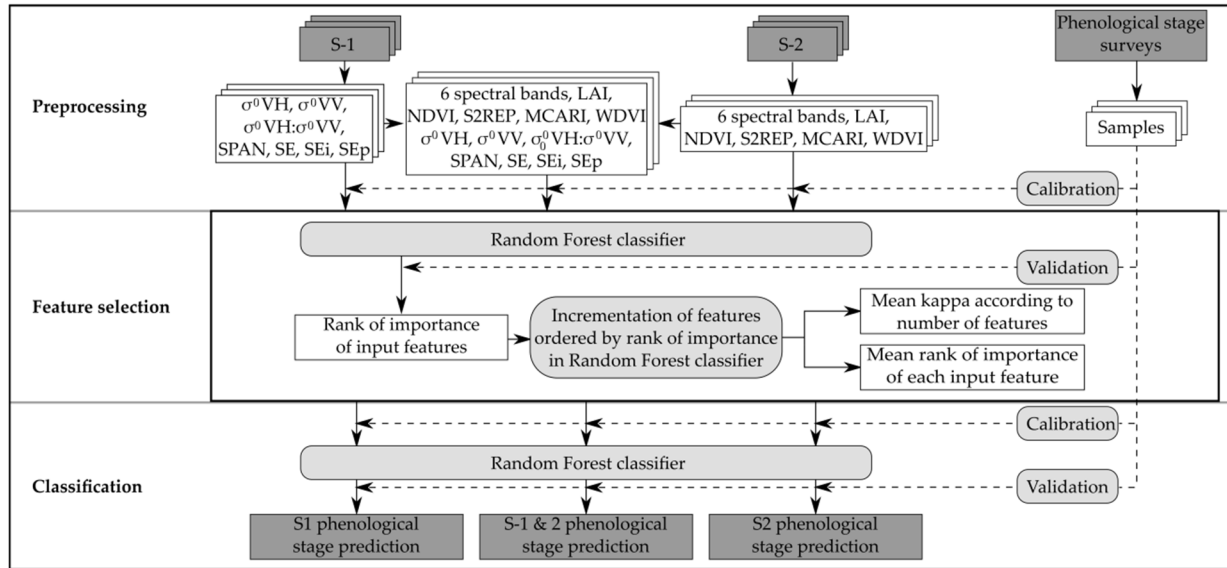


**Figure 4.** Detailed flowchart of the incremental classification procedure applied to S-1 data alone, S-2 data alone and combined S-1 & 2 data.

Incremental classification was performed using a Random Forest (RF) classifier applied to S-1 data alone, S-2 data alone, and combined S-1 & 2 data. A total set of 50 pairs of training and validation fields in a 70:30 ratio were randomly selected to classify all wheat and rapeseed phenological stages. For each of the pairs, the selected fields were the same for S-1 data alone, S-2 data alone, and combined S-1 & 2 data. A maximum number of randomly selected samples per class was set to rebalance the classes, since the RF classifier underperforms with unbalanced classes (Khoshgoftaar et al., 2007). The number of samples per pair ranged from 21 (5 principal phenological stages) or 18 (7 sub-classes of secondary phenological stages) to 52 for wheat, and from 13 to 35 for rapeseed (both types of phenological stages) (Table 6).

**Table 6.** Number of samples per pair (training + validation samples) used to classify phenological stages of wheat and rapeseed. OS = observed samples in the field, SS = selected samples for classification

Class code	Wheat fields				Rapeseed fields			
	Principal stages		Sub-classes		Principal stages		Sub-classes	
	OS	SS	OS	SS	OS	SS	OS	SS
1	105	52	49	49	18	18	18	18
2	72	52	56	52	36	35	36	35
3	21	21	72	52	38	35	12	12
4	52	52	21	21	13	13	26	26
5	35	35	52	52	44	35	13	13
6			18	18			25	25
7			17	17			19	19

Two output analysis – mean rank of importance of each input feature and mean kappa index (Cohen, 1960; Rosenfield and Fitzpatrick-Lins, 1986) as a function of the number of features – were used to select the most important features to include in the final classification. Incremental classification is used to assess mapping quality as the types and numbers of features increase. Thus, it determines the combination and number of

features in the classification necessary to obtain acceptable quality (Inglada et al., 2016). For each training and validation set (50 pairs), an RF algorithm was first applied to all of the features to rank them in order of importance based on the mean decrease in the Gini index which assessed the reliability of the incremental classification (Calle and Urrea, 2011). The mean rank of importance of each feature was derived from the 50 ranks obtained from the 50 pairs of training and validation samples. We then ran as many RF algorithms as the number of features, starting with the two most important features and then adding the less important features until all features were processed. The number of features selected for the final predictions was determined automatically: when kappa increased by less than 0.02 for three consecutive feature additions, the first of the three features marked the end of the selection for prediction. To visualize differences in performance between classes, we calculated user's accuracy (UA) and producer's accuracy (PA) (Congalton, 1991) as a function of the number of features. We used the RF algorithm to select and classify features and to calculate the final prediction. In both cases, the number of trees was set to 100 (Pelletier et al., 2016). The analysis were performed using the randomForest package of R software.

## 4. RESULTS

### 4.1 Analysis of time-series of Sentinel-2 features

For wheat and rapeseed, the highest signal variations in temporal profiles for S-2 reflectance were observed for bands 6 and 7 (red-edge) and bands 8 and 8A (near-infrared) (Fig. 5).

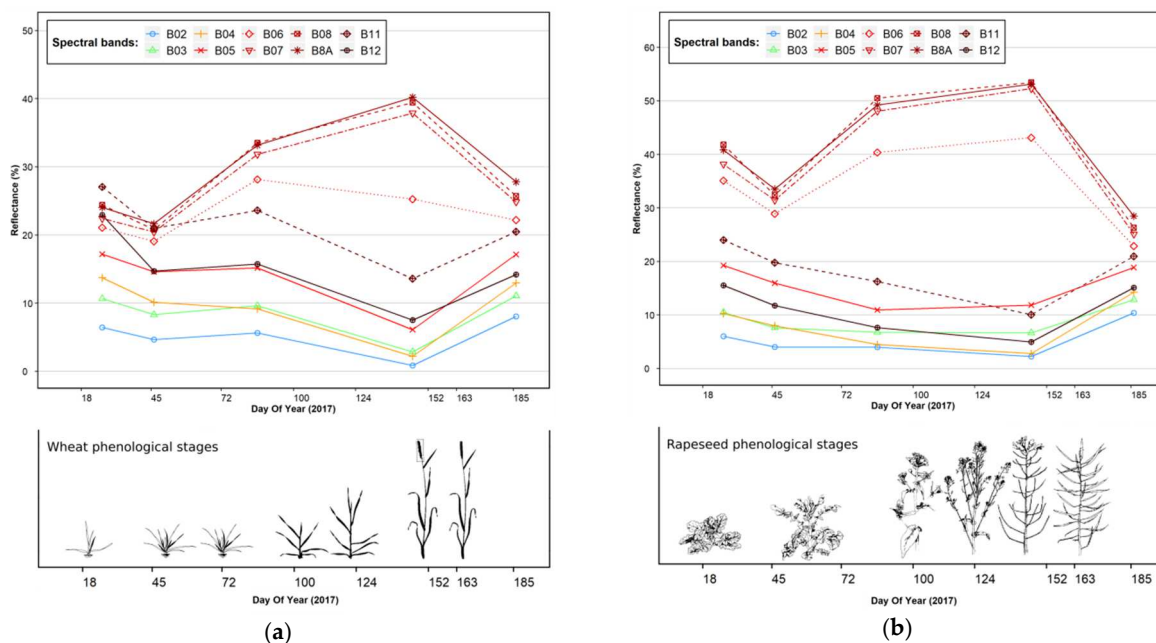


**Figure 5.** Mean temporal profiles of Sentinel-2 reflectance and main phenological stages for (a) wheat and (b) rapeseed (Bleiholder, et al., 2001) (B02 = blue, B03 = green, B04 = red, B05 = Red-edge 1, B06 = Red-edge 2, B07 = Red-edge 3, B08 = NIR wide, B8A = NIR narrow, B11= SWIR1, B12= SWIR2).

For wheat, all S-2 bands saturated before and during the maximum peak corresponding to stem elongation (DoY 100-124), inflorescence and flowering (DoY 152) (Fig. 5a). For rapeseed, all S-2 bands saturated during

flowering and development of fruit (DoY 100, BBCH stages ~ 60-65, DoY 124, BBCH stages ~67-69, and DoY 152 and 163, BBCH stage ~80) (Fig. 5b). Based on these observations, we selected S-2 bands 3, 5, 6, 7, 8 and 8A as input for the incremental classification.

In the temporal profiles of S-2-based vegetation indices and LAI for wheat and rapeseed, the standard deviation peaked on DoY 146, which corresponded to the end of inflorescence for wheat (DoY 124, BBCH stage ~55) and the end of development of fruit for rapeseed (DoY 124, BBCH stages ~67-69) (Fig. 6).

For wheat, LAI, NDVI and MCARI began to increase at the beginning of tillering, and S2REP and WdVI at the end of tillering. They all decreased during ripening.

For rapeseed, decreases are observed during ripening. NDVI increased until the development of fruit. However, it is not possible to observe its saturation due to the poor number of S-2 dates. LAI and WdVI were similar: they began to increase at the beginning of inflorescence (DoY 46) until the beginning of flowering (DoY 86). WdVI was the only vegetation index sensitive to leaf development (DoY 18-45).

For both crop types, MCARI had a high standard deviation. Thus, MCARI can produce inaccurate predictions of phenological stages.

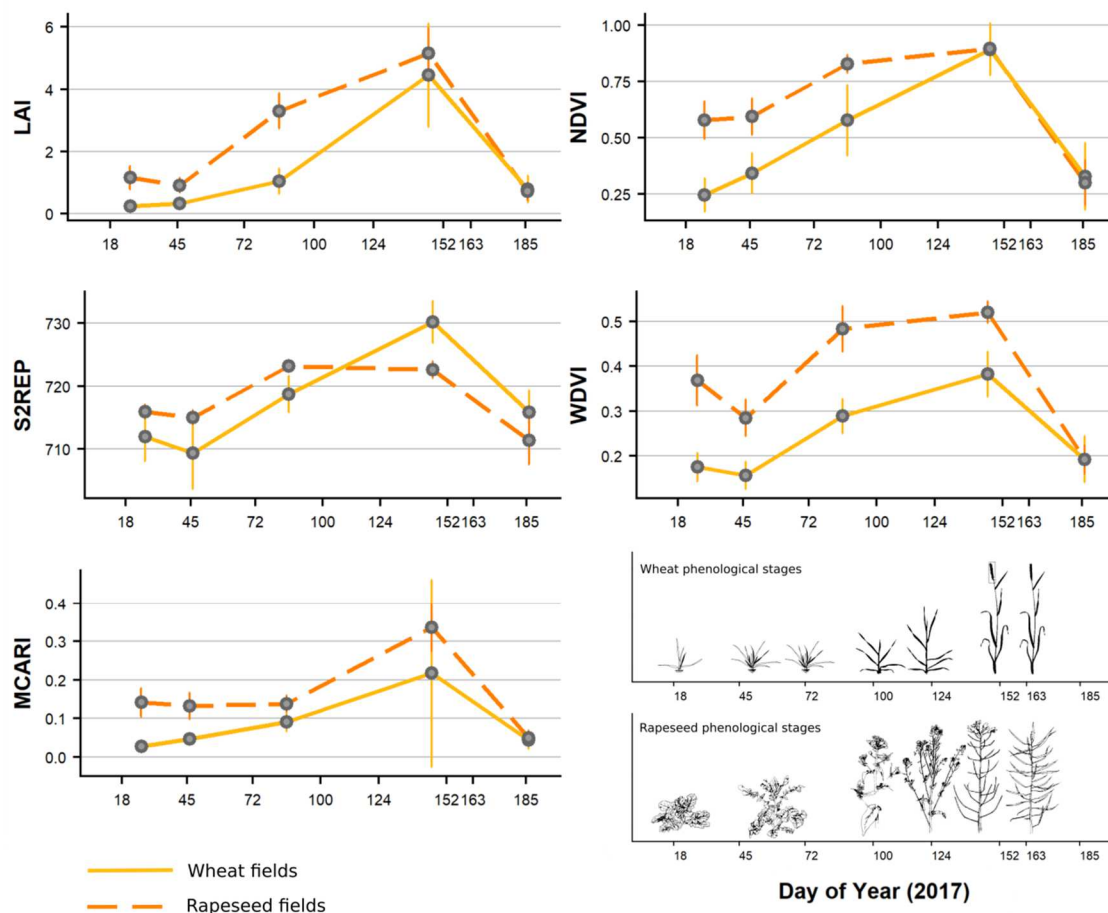


**Figure 6.** Mean temporal profiles of Sentinel-2 vegetation indices and LAI and main crop phenological stages for wheat and rapeseed (Bleiholder, et al., 2001) (NDVI = Normalized Vegetation Index, S2REP = S-2 Red-Edge Position index, MCARI = Modified Chlorophyll Absorption in Reflectance Index, WdVI = Weighted Difference Vegetation Index, LAI = Leaf Area Index). Error bars indicate 1 standard deviation.

## 4.2 Analysis of time series of Sentinel-1 features

For wheat, while trends in the temporal profiles for  $\sigma^{0VH}$  and  $\sigma^{0VV}$  were similar,  $\sigma^{0VV}$  was influenced more by wheat growth than  $\sigma^{0VH}$  (Fig. 7). Both polarizations increased during tillering (DoY 18-72). Both  $\sigma^{0VH}$  and  $\sigma^{0VV}$  decreased throughout stem elongation (DoY 72-124) but increased from inflorescence to ripening. The  $\sigma^{0VH}:\sigma^{0VV}$  ratio has varied little during tillering stages. The ratio increased strongly during stem elongation and slightly from the beginning of inflorescence to ripening. The polarimetric indices were also sensitive to wheat phenological stages, according to their temporal behaviors (Fig. 7). The temporal behaviors of  $SPAN$ ,  $\sigma^{0VH}$  and  $\sigma^{0VV}$  were similar. The normalized SE index and its intensity ( $SE_i norm$ ) were similar. The influence of polarization ( $SE_p norm$ ) on SE was weak, with values ranging from -0.9 to 0.8 dB, while  $SE_i norm$  ranged from -5 to -1 dB.  $SE norm$  and  $SE_i norm$  initially increased at tillering but then decreased during stem elongation and inflorescence.  $SE_p norm$  initially varied little but then significantly increased during stem elongation.  $SE_p norm$  decreased linearly from the end of flowering to ripening.

For rapeseed, the trends for  $\sigma^{0VH}$  and  $\sigma^{0VV}$  were similar, showing that they were sensitive to phenological stages, while the  $\sigma^{0VH}:\sigma^{0VV}$  ratio was affected only slightly (Fig. 7). VH and VV polarizations increased slightly during leaf development, varied little during inflorescence and decreased during flowering. Both polarizations increased from development of fruit to the beginning of ripening. They decreased until the end of ripening. Like for wheat, the temporal profiles of span,  $\sigma^{0VH}$  and  $\sigma^{0VV}$  for rapeseed were similar.  $SE_p norm$  varied little throughout the rapeseed cycle. Temporal changes in  $SE norm$  and  $SE_i norm$  were similar to those of wheat,  $SE_i norm$  increased during flowering and decreased during ripening.

SAR S-1 features were more sensitive to the development of fruit stage for rapeseed (Fig. 7) than optical S-2 features, which saturated from development of fruit (DoY 86) to beginning of ripening (DoY 163) (Fig. 5 and 6).

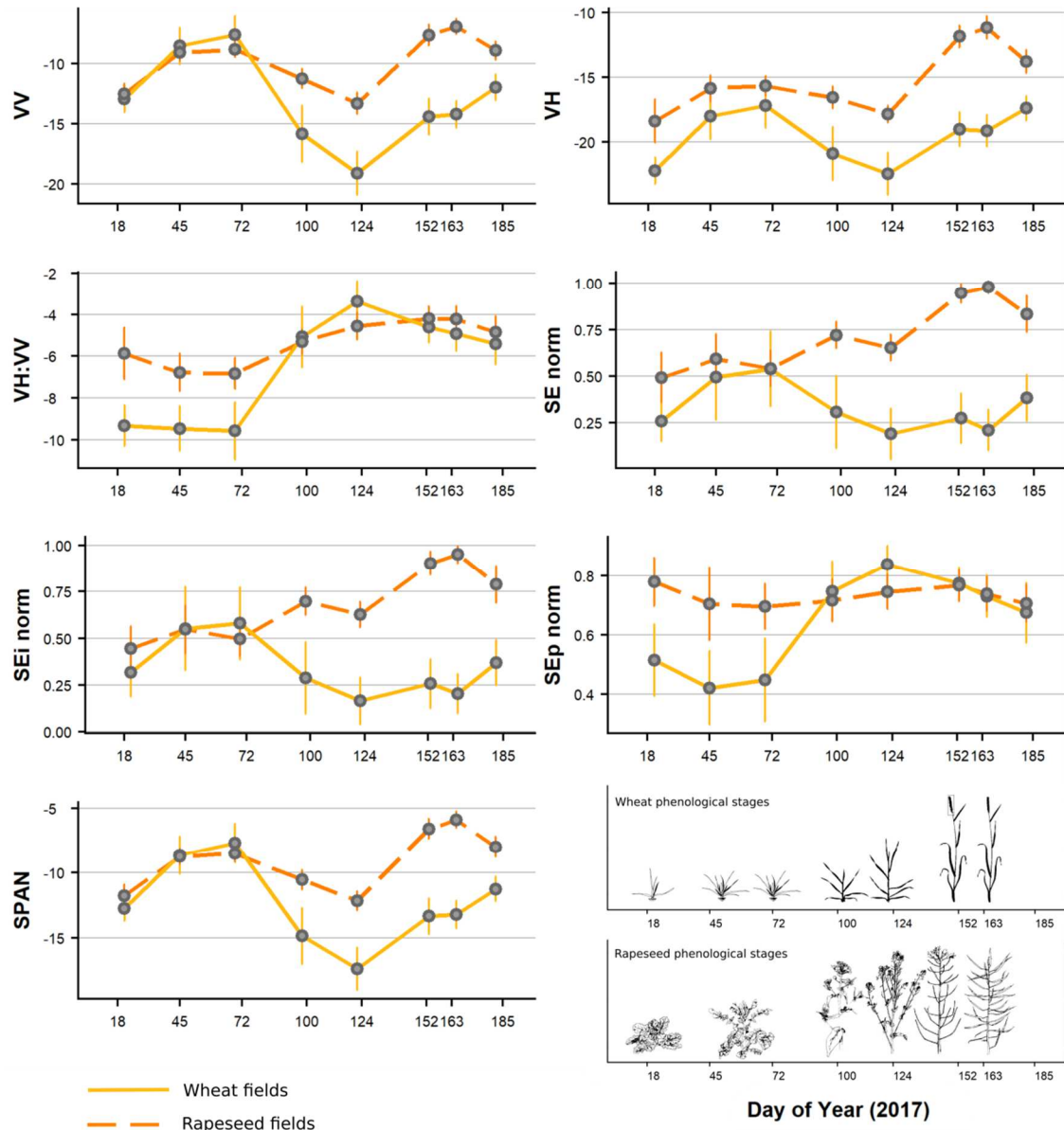


**Figure 7.** Mean and standard deviation of the Sentinel-1 backscattering coefficients and polarimetric indicators and main crop phenological stages for wheat and rapeseed (Bleiholder, et al., 2001) ( $VH = \sigma^0 VH$ ,  $VV = \sigma^0 VV$ ,  $VH:VV = \sigma^0 VH : \sigma^0 VV$ ,  $SPAN =$  total scattered power,  $SE_i norm =$  normalized Shannon entropy,  $SE_i norm =$  normalized Shannon entropy Intensity,  $SE_p norm =$  normalized Shannon entropy Polarization). Error bars indicate 1 standard deviation.

### 4.3 Contribution of Sentinel 1 & 2 time series to monitoring wheat and rapeseed phenology

#### 4.3.1 Contribution of Sentinel 1 & 2 time series to identifying principal phenological stages of wheat and rapeseed

The combined use of S-1 & 2 data outperformed use of S-1 or S-2 data alone in detecting the principal crop stages of wheat and rapeseed (maximum mean kappa index of 0.82 and 0.91, respectively) (Fig. 8). However, considering the standard deviation of the mean kappa index, results of the combined use of S-1 & 2 data were similar to those of S-2 data alone. The number of features automatically selected to predict the principal phenological stages were 4, 6 and 6 for wheat and 4, 5 and 5 for rapeseed for S-1 data alone, S-2 data alone and



their combined use, respectively. For wheat, the mean kappa indices of S-1 and S-2 data alone were equal up to 3 input features, after which the S-1 mean kappa index changed little ( $0.60 \pm 0.07$ ), while that for S-2 continued to increase up to 5 input features ( $0.74 \pm 0.07$ ) (Fig. 8a). Using the top 6 S-1 & 2 features out of all 18 features increased the mean kappa index by ca. 0.24 (i.e. from  $0.53 \pm 0.11$  for 2 features to  $0.77 \pm 0.07$  for 6 features). For rapeseed, S-1 data alone underperformed S-2 data alone based on the standard deviation of the mean kappa index (Fig. 8b). Using the top 5 S-1 & 2 features out of all 18 features increased the mean kappa index by ca. 0.16 (i.e. from  $0.74 \pm 0.12$  for 2 features to  $0.90 \pm 0.07$ ).

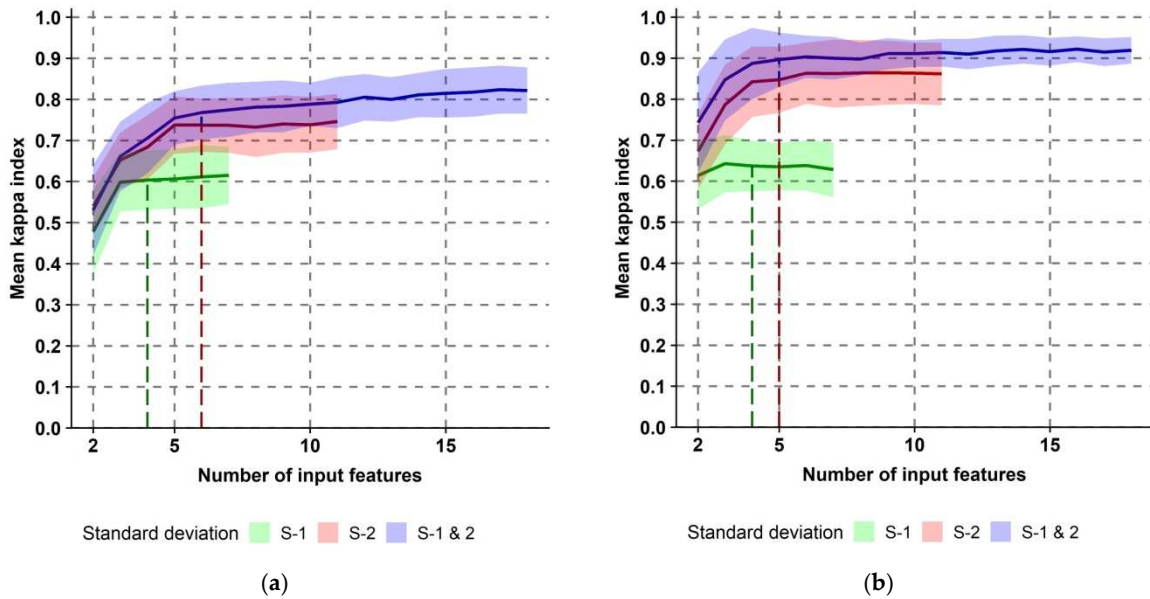


**Figure 8.** Mean kappa index of incremental classifications of principal phenological stages for Sentinel-1 data alone, Sentinel-2 data alone, and combined Sentinel-1 & 2 data as a function of the number of input features for (a) wheat and (b) rapeseed. The dashed lines indicate the number of features automatically selected for the predictions. The combined use of S-1 & 2 data outperformed use of S-1 or S-2 data alone in detecting the principal crop stages of wheat and rapeseed.

When using S-2 data alone for wheat (Fig. 9b), LAI was the most important feature, followed by S2REP, red-edge2 (B06) and WDV, NDVI and red edge1 (B05). For rapeseed (Fig. 9e), the top 3 features were NDVI, S2REP and band 3 (green) (mean ranks of 1.4, 2.1 and 4 respectively). They were followed by LAI and WDV (mean ranks of 4.3 and 5.3 respectively).

When using S-1 data alone, the  $\sigma^{0}VH:\sigma^{0}VV$  ratio ranked first for both crops, while  $\sigma^{0}VV$  ranked third for wheat (Fig. 9a and 9d). Polarimetric indicators were important for wheat and rapeseed: several of them were among the 4 input features selected for predictions for both crops. For wheat, the polarization of the SE ( $SE_p norm$ ) ranked second (Fig. 9a), for rapeseed, the intensity of the SE ( $SE_i norm$ ) ranked fourth (Fig. 9d).

When using combined S-1 & S2 data, an S-1 feature was the most important for both crops:  $\sigma^{0}VH:\sigma^{0}VV$  for wheat (Fig. 9c) and  $\sigma^{0}VH$  for rapeseed (Fig. 9f). Among the top 10 important features, 6 were S-1 features for both crop types. For S-2 features, LAI was the most important for wheat and the NDVI and S2REP for rapeseed, since they were the only features out of the 6 and 5 features selected for prediction using the combined use of S-1 & 2 data. MCARI was the least important S-2 index for both crops.

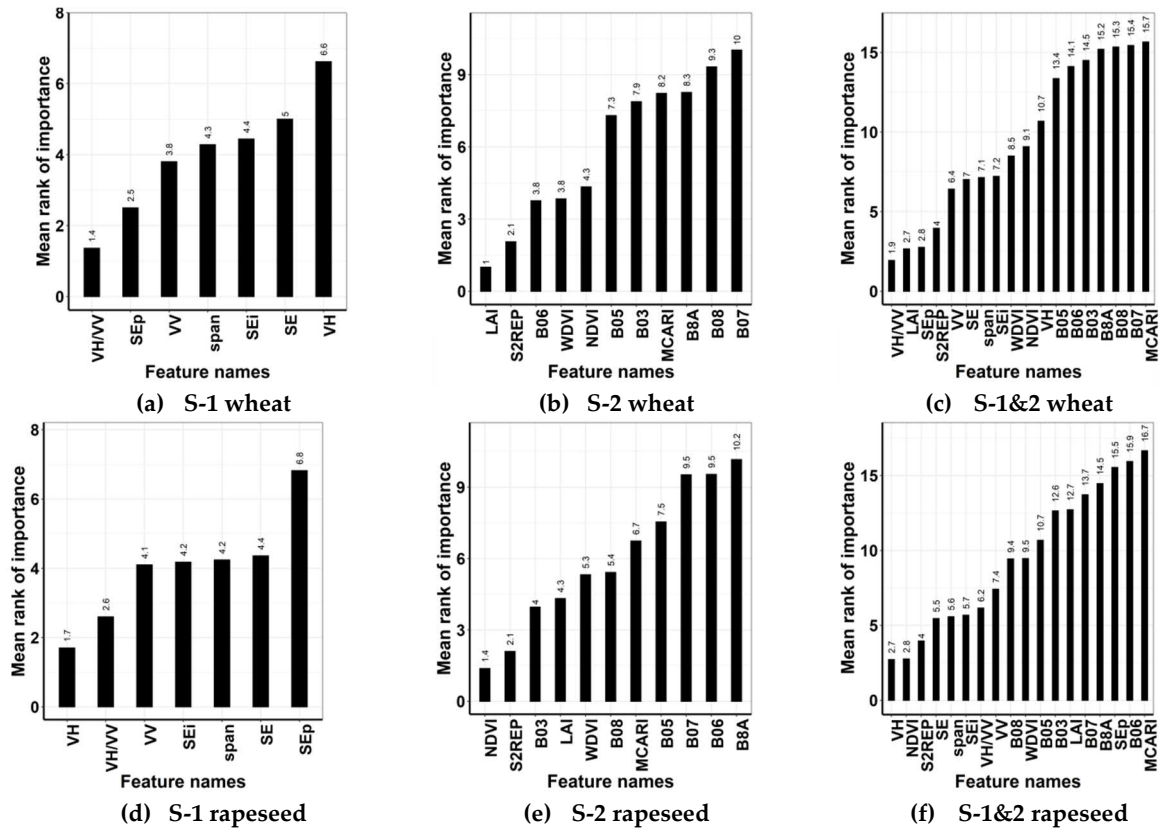


**Figure 9.** Mean rank of importance of the most important features to identify the 5 principal phenological stages of (a, b, c) wheat and (d, e, f) rapeseed for (a, d) Sentinel-1 data alone, (b, e) Sentinel-2 data alone and (c, f) combined Sentinel-1 & 2 data. The  $\sigma^0VH:\sigma^0VV$  ratio was a relevant feature using S-1 data alone for both crops, while LAI and NDVI were the most important features using S-2 data alone for wheat and rapeseed, respectively.

Concerning classification results for wheat, tillering was the phenological stage most accurately classified using S-1 data alone, S-2 data alone and their combined use (Fig. 10a-c and 11a-c). Based on the UA and PA results, similar results were obtained using S-1 or S-2 data alone for the stem elongation stage. The tillering stage was identified better using S-1 than S-2 data, while the flowering, development of fruit and ripening stages were identified better using S-2 than S-1 (Fig.10a and 10b). Combined use of S-1 & 2 data improved the UA of tillering, stem elongation and ripening; only the PA of the stem elongation and flowering stages underperformed that of S-2.

For rapeseed, development of fruit was the most difficult phenological stage to identify using S-1 data alone and the combined use of S-1 & 2 data, due to confusion with ripening (Appendix B, Table B4 and B6 and Fig. 10d and 10f, 11d and 11f). S-2 data alone provided better results than S-1 data alone for all classes (Fig 10d-e, 11d-e), while their combined use improved the PA of the leaf development stage from 0.8 (S-2) to 1 (S-1 & 2) (Fig. 10e-f, 11e-f).

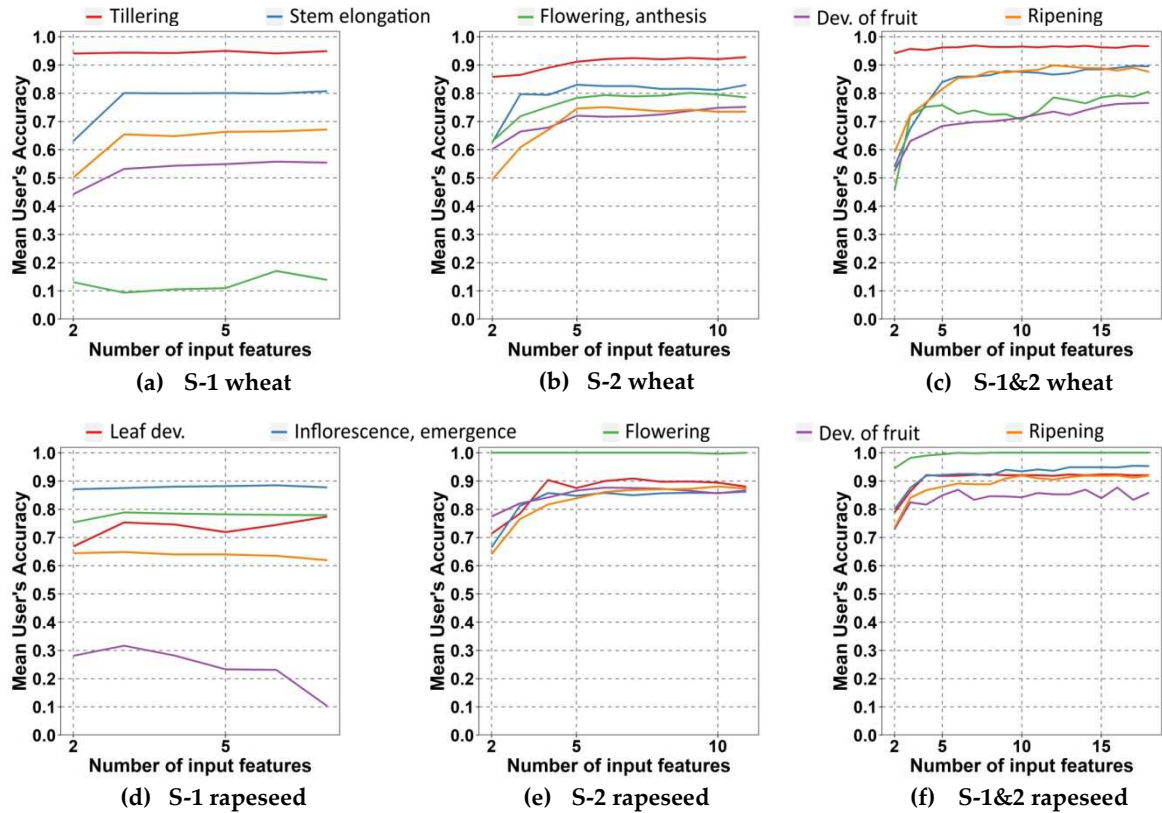


**Figure 10.** Mean user's accuracy (UA) of incremental classifications as a function of the number of input features to identify the 5 principal phenological stages of wheat and rapeseed. The colored lines refer to the crop phenological stages.

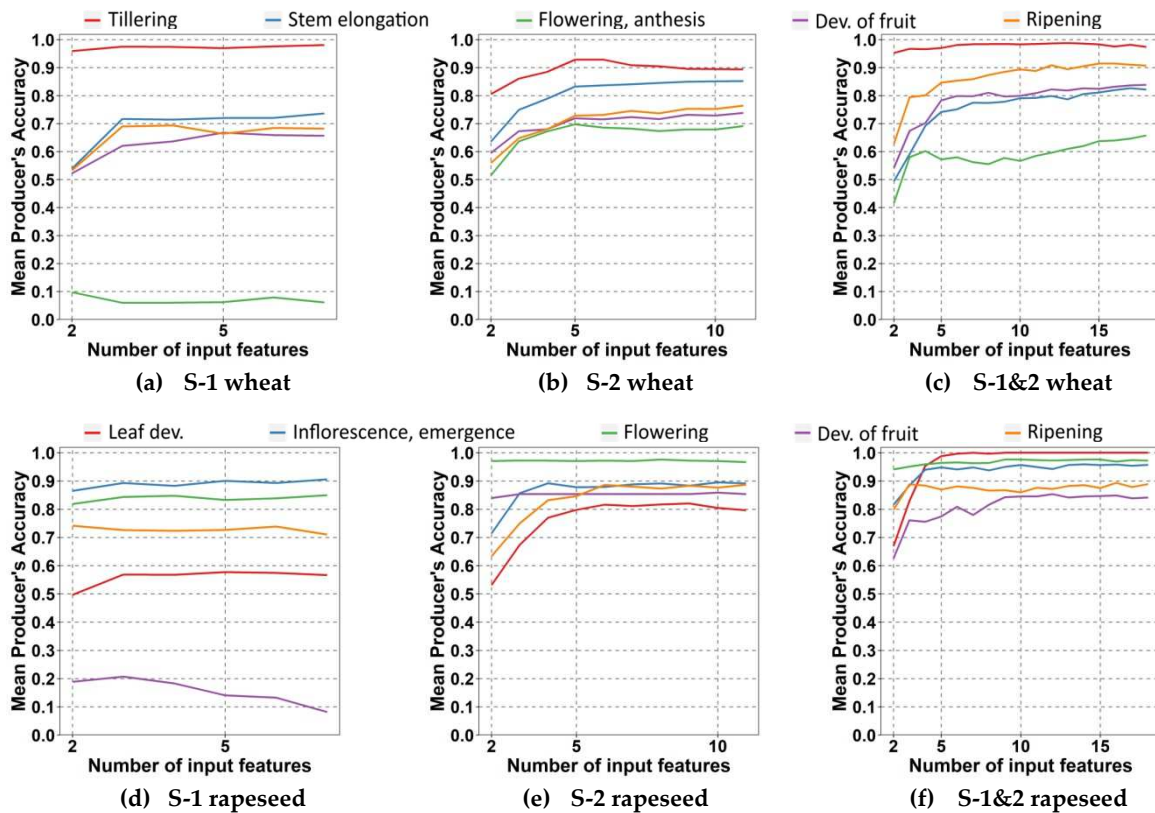


**Figure 11.** Mean producer's accuracy (PA) of incremental classifications as a function of the number of input features to identify the 5 principal phenological stages of wheat and rapeseed. The colored lines refer to the crop phenological stages.

#### 4.3.2 Contribution of Sentinel 1 & 2 time series to identifying secondary phenological stages of wheat and rapeseed

The number of features automatically selected to predict secondary phenological stages were 4, 4 and 7 for wheat (Fig.12a) and 4, 4 and 5 for rapeseed (Fig. 12b) for S-1 data alone, S-2 data alone and their combined use, respectively. For S-2 data alone, the mean kappa indices of wheat were similar to those for the principal phenological stages using the number of features automatically selected ( $0.72 \pm 0.05$  and  $0.74 \pm 0.06$ ), whereas the secondary phenological stages of rapeseed were identified weaker than principal phenological stages ( $0.77 \pm 0.07$  and  $0.86 \pm 0.07$ , respectively). S-1 data alone did not discriminate secondary phenological stages well, since their mean kappa indices were significantly lower than those for the principal phenological stages ( $0.53 \pm 0.06$  and  $0.60 \pm 0.07$ , respectively, for wheat and  $0.55 \pm 0.07$  and  $0.63 \pm 0.06$ , respectively, for rapeseed). For combined S-1 & 2 data, mean kappa indices for secondary phenological stages were also lower than those of principal phenological stages ( $0.72 \pm 0.07$  and  $0.77 \pm 0.06$ , respectively, for wheat and  $0.79 \pm 0.06$  and  $0.9 \pm 0.07$ , respectively, for rapeseed). The use of S-1 & 2 data combined was similar to those of S-2 data alone for both crops (Fig. 12a and 12b). Several S-1 features were present in the top ranks of importance for the combined S-1 & 2 data (Fig. 13c and 13f). Considering standard deviation of the mean kappa index, the classification accuracy using S-2 data alone or combined S-1 & 2 was not significantly different. For rapeseed, the mean kappa index was very similar regardless of the number of input features. For wheat, S-2 data alone results were superior to combined S-1 & 2 results until 5 inputs features.

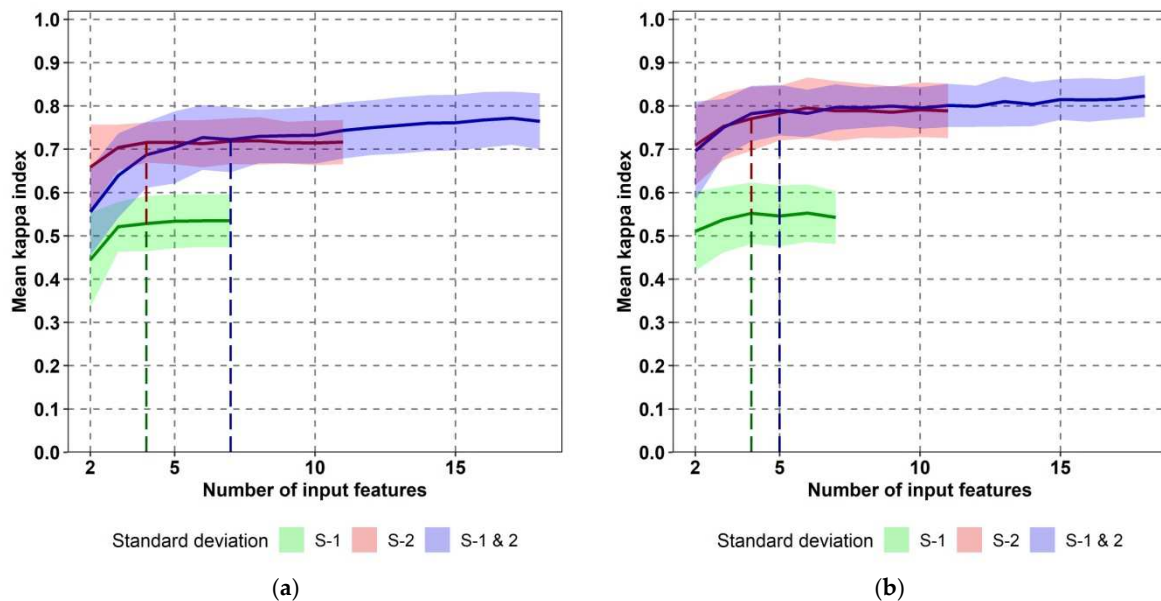


**Figure 12.** Mean kappa index of incremental classifications of secondary phenological stages for Sentinel-1 data alone (green), Sentinel-2 data alone (red), and combined Sentinel-1 & 2 data (blue) as a function of the number of input features for (a) wheat and (b) rapeseed. The classification accuracy using S-2 data alone or combined S-1 & 2 was not significantly different.

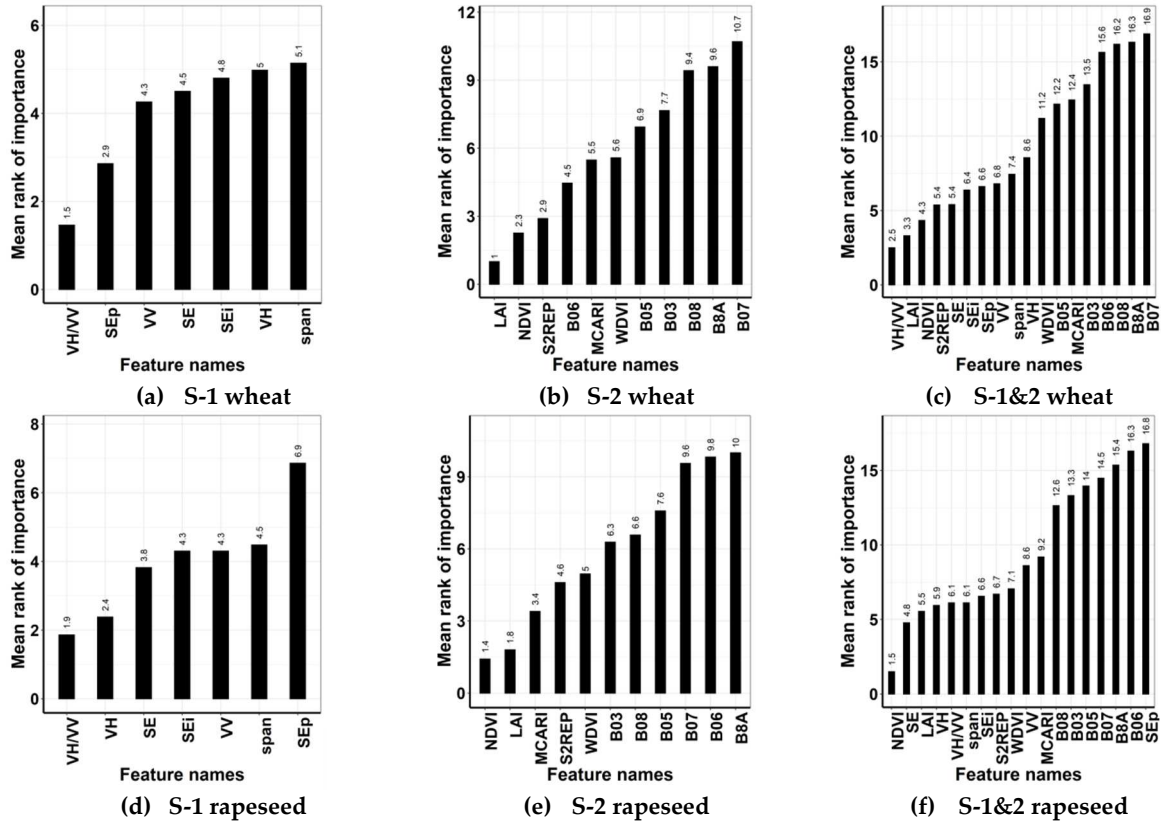


**Figure 13.** Mean rank of importance of the most important features to identify the 7 secondary phenological stages of wheat and rapeseed. The  $\sigma^{0VH}:\sigma^{0VV}$  ratio was the most important feature using S-1 data alone for both crops, while LAI, NDVI and S2REP were the most important features using S-2 data alone.

When using S-2 features alone, LAI, NDVI and S2REP for both crop types remained, like those for the principal phenological stages, the most important features (Fig. 11e and 13e). For rapeseed, band 3 (green), which had been ranked third for identifying the principal phenological stages (Fig. 10e) decreased to the sixth rank for identifying the secondary phenological stages (Fig. 13e).

The  $\sigma^{0VH}:\sigma^{0VV}$  ratio was the most important feature using S-1 data alone for both crops (Fig. 13a and 13d), and the first and seventh feature using S-1 & 2 data combined (Fig. 13c and 13f) for wheat and rapeseed, respectively.

When using S-1 features alone,  $\sigma^{0VV}$  and  $SE_p norm$  for wheat (Fig. 13a) and  $\sigma^{0VV}$  and  $SE norm$  for rapeseed (Fig. 13d) were also highly important for identifying secondary phenological stages.  $SE norm$  appeared more important for discriminating secondary phenological stages than principal phenological stages, increasing by 3 ranks for both crops, while the rank of span decreased from third and first for wheat and rapeseed, respectively.



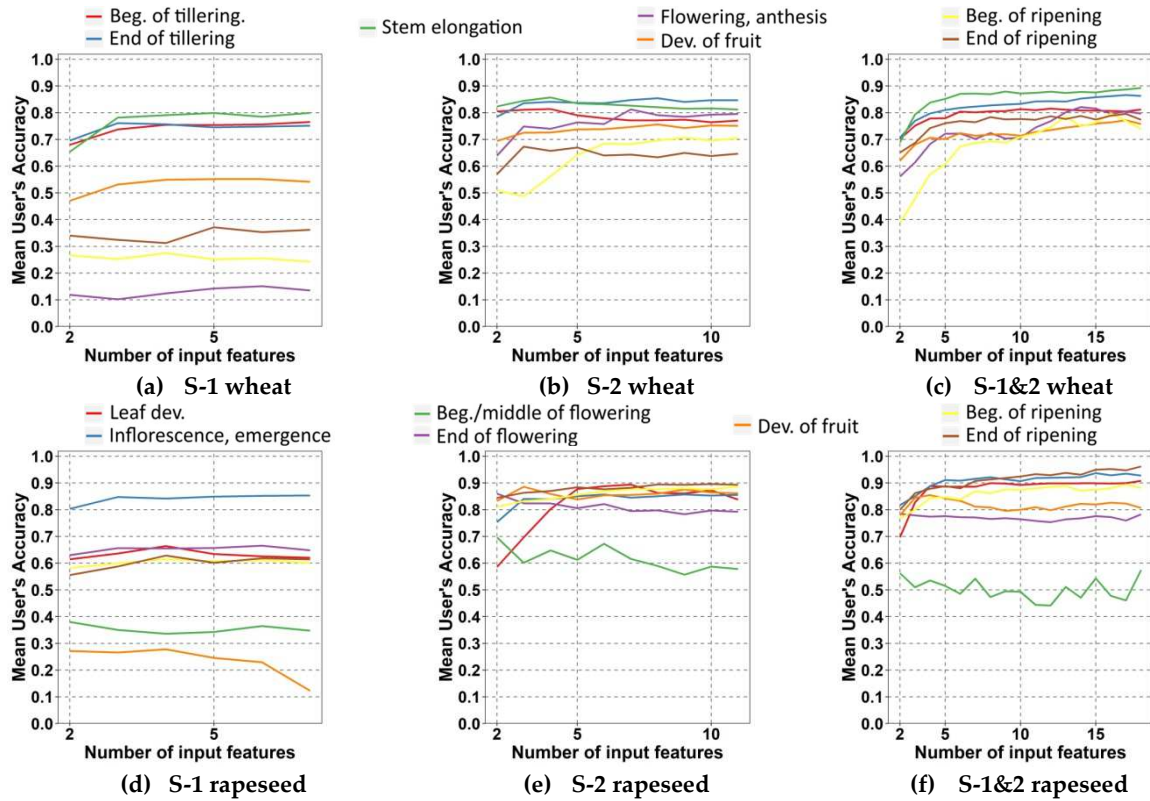


**Figure 14.** Mean user's accuracy of incremental classifications as a function of the number of input features to identify the 7 secondary phenological stages of wheat and rapeseed. The colored lines refer to these secondary phenological stages.

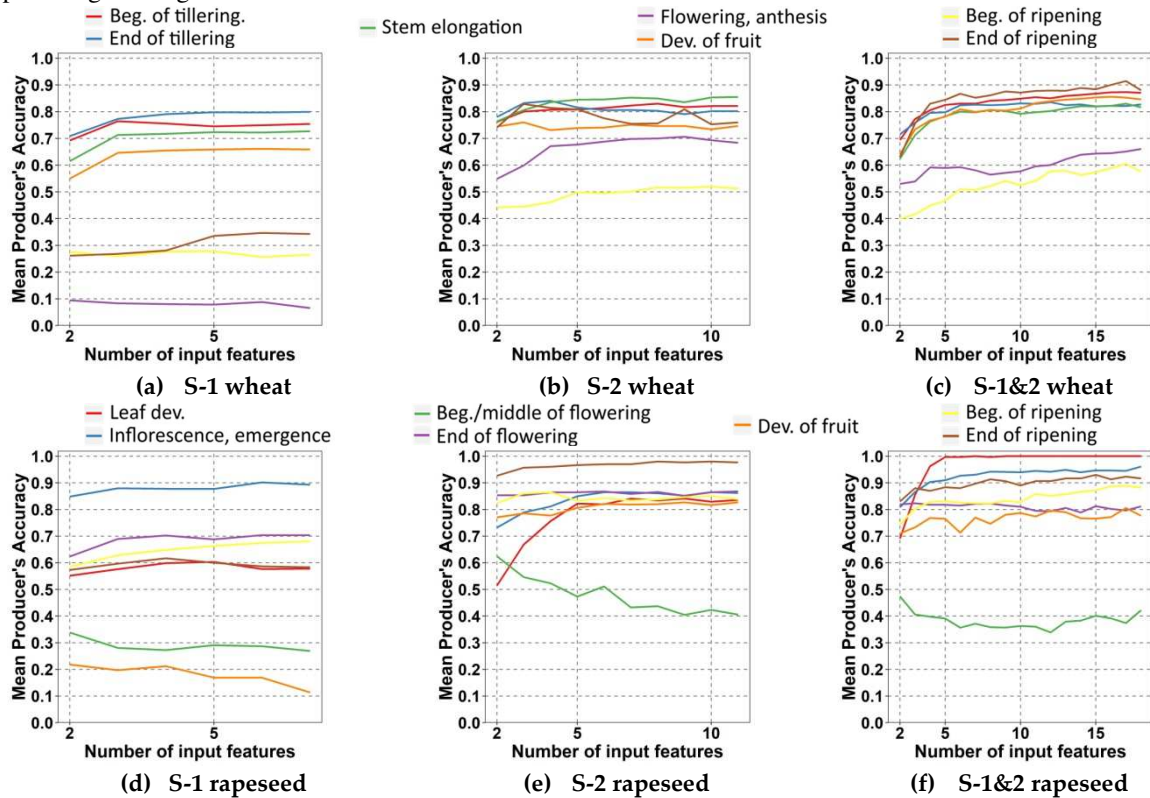


**Figure 15.** Mean producer's accuracy of incremental classifications as a function of the number of input features to identify the 7 secondary phenological stages of wheat and rapeseed. The colored line refer to the secondary phenological stages.

For classification results for wheat, S-1 data alone (Fig. 14a and 15a) underperformed S-2 data alone (Fig. 14b and 15b) and combined S-1 & 2 data (Fig. 14c and 15c) in classifying flowering, development of fruit and the beginning and end of ripening. However, by combining S-1 & 2 features (Fig. 14c and 15c), the accuracy of the secondary phenological stages was either similar to those of S-2 data alone (Fig. 14b and 15b) or higher, except for the flowering and the end of ripening stages based on the PA.

For classification results for rapeseed, the leaf development, the beginning/middle of flowering and the end of development of fruit were the stages least well predicted using S-1 data alone (Fig. 14d and 15d) or S-2 data alone (Fig. 14e and 15e). Combined use of S-1 & 2 data increased the accuracy of identifying the leaf development stage (Fig. 14f and 15f).

## 5. DISCUSSION

### 5.1 *The relationship between Sentinel-2 features and phenological stages of wheat and rapeseed*

For both crop types, the temporal profiles of S-2 bands were consistent with those observed by Ashourloo et al (2019). Saturation was observed from stem elongation to flowering for wheat and from flowering to development of fruit for rapeseed (Fig.5). However, it should be noted that the analysis of the temporal profiles was done from only 5 dates due to the heavy cloud cover over the study area between DOY 72 and 152, i.e. during the stem elongation, booting and early flowering stages for wheat and the flowering and development of fruit stages for rapeseed. Wilson et al. (2014) mentioned signal saturation for wheat and rapeseed when using hyperspectral data within a 400-900 nm range and identified optimal bands for identifying crops in green, red-edge and near-infrared wavelengths. Based on this study and our observations, we selected S-2 bands 3, 5, 6, 7, 8 and 8A as input for the incremental classification

In the temporal profiles of S-2-based vegetation indices and LAI, the standard deviation peaked at the end of inflorescence for wheat and the end of development of fruit for rapeseed (Fig. 6). Thus, the heterogeneity in crop phenology among fields during the field surveys peaked earlier during the middle of stem elongation for wheat and the beginning of development of fruit for rapeseed. All vegetation indices saturated when the LAI was high (1-2 for wheat and 3-4 for rapeseed, depending on the vegetation index), which confirms observations of Haboudane et al. (2004) for wheat.

For wheat, the vegetation indices and LAI began to increase when the chlorophyll content increased at the tillering stage. They all decreased during ripening, as plants dried.

For rapeseed, decreases are observed during ripening due to the decrease in chlorophyll content as plants dried. LAI and WDVI began to increase at the beginning of inflorescence until the beginning of flowering as plant area expanded. WDVI decreased during the leaf development as leaves unfolded.

## 5.2 The relationship between Sentinel-1 backscatter coefficients and phenological stages of wheat and rapeseed

For wheat, while trends in the temporal profiles for  $\sigma^{0VH}$  and  $\sigma^{0VV}$  were similar,  $\sigma^{0VV}$  was higher than  $\sigma^{0VH}$  especially during the first phenological stages (i.e. tillering and stem elongation), since  $\sigma^{0VV}$  is influenced more by wheat growth than  $\sigma^{0VH}$  (Fig. 7). This is consistent with observations of Cookmartin et al. (2000) who showed that  $\sigma^{0VV}$  is particularly sensitive to vegetation wetness and of Fieuzal et al (2013) who observed maximum water content at the stem elongation stage. Both polarizations increased during tillering (DoY 18-72). The increase in the number of stems per plant and the length of stems results in an increase in VH polarization, which is dominated by double-bounce and volume-scattering mechanisms (Lopez-Sanchez et al., 2013; Wiseman et al., 2014; Veloso et al., 2017) and a strong increase in VV polarization, which is dominated by the influence of soil and canopy. Both  $\sigma^{0VH}$  and  $\sigma^{0VV}$  decreased throughout stem elongation but increased from inflorescence to ripening, as observed by Fieuzal et al. (2013), due to an increase in crop absorption when vegetation was wet, and decreased as vegetation dried. VV polarization is attenuated by vertical transformation of the structure of wheat during stem elongation (Brown et al., 2003). The  $\sigma^{0VH}:\sigma^{0VV}$  ratio has varied little during tillering stages, which does not help identify secondary phenological stages. This ratio correlates more to fresh biomass than to photosynthetic activity (Veloso et al., 2017). For rapeseed, VH and VV polarizations increased slightly during leaf development as biomass increased. They varied little during inflorescence and decreased during flowering. Indeed, rapeseed's vertical transformation from a thick rosette of leaves to a flowering stalk attenuated VV polarization, while its low density attenuated VH polarization. Both polarizations increased from development of fruit to the beginning of ripening, which was also observed in other studies (Fieuzal et al., 2013; Lopez-Sanchez et al., 2013; Wiseman et al., 2014; Veloso et al., 2017). The progressive development of structure without preferred orientations results in a more complex geometry, inducing a strong increase in the volume-scattering mechanism (Betbeder et al., 2016). VH and VV polarizations decreased until the end of ripening due to the decrease in water content in the top layer of rapeseed. VV polarization is particularly sensitive to the water content of vegetation (Cookmartin et al., 2000), and VH is attenuated by the increase in wave penetration into the soil.

## 5.3 The relationship between Sentinel-1 polarimetric indicators and phenological stages of wheat and rapeseed

For both crop types, the temporal behaviors of  $SPAN$ ,  $\sigma^{0VH}$  and  $\sigma^{0VV}$  were similar since span is the total scattered power. For wheat,  $SE\ norm$  and  $SE_i\ norm$  initially increased at tillering but then decreased during stem elongation and inflorescence. The increase in  $SE_i\ norm$  was related to stem development during tillering. This complexity of plant structure increased the disorder encountered in the radar signal. The opposite was observed during stem elongation, due to the less complex structure of wheat, which resulted in a decrease in backscatter power. Betbeder et al. (2016) demonstrated a strong positive correlation ( $r^2=0.7$ ) between topsoil moisture and  $SE_i$  during leaf development and tillering due to a low wave penetration into the soil.  $SE_p\ norm$  initially varied little but then significantly increased during stem elongation, indicating that polarization varied greatly due to heterogeneity in plant structures in wheat fields.  $SE_p\ norm$  decreased linearly from the end of



flowering to ripening, as wheat was becoming homogeneous at the field scale.  $SE\ norm$  and  $SE_i\ norm$  could identify the development of fruit stage, unlike the other S-1 features, since they decreased slightly during this stage. For rapeseed, the temporal changes in  $SE\ norm$  and  $SE_i\ norm$  were similar to those of wheat. As mentioned by Betbeder et al. (2016), the intensity of SE was sensitive to different phenological stages. The slight increase in  $SE_p\ norm$  during flowering was associated with changes in rapeseed structure from a thick rosette of leaves to a flowering stalk, resulting in a strong variation in backscattering polarization (Betbeder et al., 2016).  $SE_i\ norm$  increased as rapeseed biomass increase; thus, it increased during flowering and decreased during ripening (Betbeder et al., 2016).

#### 5.4 Relative contributions of S-1 and S-2 data to mapping of wheat and rapeseed phenological stages

Concerning the prediction of principal phenological stages of wheat using S-2 data alone (Fig. 9b), LAI was the most important feature, followed by S2REP, red-edge2 (B06) WDV, NDVI and red edge1 (B05). For rapeseed (Fig. 9e), the most important 5 features were NDVI, S2REP, band 3 (green), LAI and WDV. Principal and secondary phenological stages of wheat and rapeseed were well identified by LAI derived from S-2 data, since this index is related to the density of green vegetation. The incremental classification results demonstrated the relevance of the S2REP index for both crop types, which is consistent with results of Frampton et al. (2013). S2REP, which is highly sensitive to chlorophyll content, is calculated from red-edge bands of S-2 that respond to high large changes in leaf reflectance (Hatfield et al., 2008). The importance of the S-2 red-edge bands has been demonstrated for predicting green LAI in crop fields, including wheat in Spain and Germany (Delegido et al., 2011). We noted the potential of WDV for predicting rapeseed phenology based on our analysis of temporal profiles; it was the only index sensitive to the leaf development stage. Wilson et al. (2014) explained that rapeseed had higher reflectance in the green and red portions of the spectrum than other crops because of its yellow flowers.

Concerning principal and secondary phenological stages classification of wheat using S-1 data alone, the  $\sigma^0VH:\sigma^0VV$  ratio ranked first for both crops, while  $\sigma^0VV$  ranked third (Fig. 9a and 9d). Previous studies demonstrated the suitability of backscattering coefficients ( $\sigma^0VH$ ,  $\sigma^0VV$ ) and the polarization ratio ( $\sigma^0VH:\sigma^0VV$ ) for estimating biomass and LAI of wheat (Dente et al., 2008; Jin et al., 2015; Betbeder et al., 2016) and maize (Gao et al., 2013). Veloso et al. (2017) concluded that the influence of the ground was similarly reduced for wheat using  $\sigma^0VH:\sigma^0VV$  compared to  $\sigma^0VH$  and  $\sigma^0VV$ , and was generally more consistent for wheat and rapeseed. For rapeseed, the  $\sigma^0VH:\sigma^0VV$  ratio was the most important feature using S-1 data alone for classify principal and secondary phenological stages. The  $\sigma^0VH:\sigma^0VV$  ratio had shown high performance in identifying principal phenological stages of both crops, confirming its high reliability for identifying principal and secondary phenological stages.

Consistent with results of Betbeder et al. (2016), polarimetric indicators were important for wheat and rapeseed: several of them were among the 4 input features selected based on the threshold automatically defined for predictions of principal and secondary phenological stages for both crops. SEp and span were selected to

predict principal phenological stages of wheat and SE<sub>i</sub> was selected for rapeseed, while for secondary phenological stages, the selection included SE<sub>p</sub> and SE for wheat and SE<sub>i</sub> and SE for rapeseed.

This study aimed to evaluate the potential of S-1 data alone, S-2 data alone, and their combined use to predict wheat and rapeseed phenological stages. For wheat, the combined use of S-1 & 2 data outperformed use of S-1 or S-2 data alone in detecting the principal phenological stages of wheat and rapeseed. The secondary phenological stages of wheat were identified better using S-2 than S-1 data. Based on the standard deviation of the mean kappa index, similar results were obtained using S-2 data alone or combined S-1 & 2 data for the secondary phenological stages of wheat. The tillering was the principal and secondary phenological stage most accurately classified using S-1 data alone, S-2 data alone and their combined use (Fig. 10a-c and 11a-c). From DOY 18 to 72, wheat was at tillering stage and a specific temporal behavior of S-1 and S-2 features was observed in comparison to all other phenological stages. However, the tillering stage was identified better using S-1 than S-2 data, while the flowering, development of fruit and ripening stages were identified better using S-2 than S-1 (Fig.10a and 10b). The SAR signal is sensitive to the geometry (e.g. roughness, texture, internal structure) and wetness of the observed targets, while optical reflectance is influenced by their physiology. Thus, we can conclude that the tillering stage of wheat was better discriminated by the structure of the wheat field rather than its physiology. From the stem elongation stage, the geometry of the wheat became vertical and varied little until ripening, while chlorophyll content increased and then decreased. Thus, S-2 features were more efficient than S-1 features to discriminate these phenological stages of wheat. For principal phenological stages of wheat, combined use of S-1 & 2 data improved the UA of tillering, stem elongation and ripening; only the PA of the stem elongation and flowering stages underperformed that of S-2. This is consistent with previous studies that have shown saturation of the C-band (El Hajj et al., 2019) and optical bands (Haboudane et al., 2004) at high levels of wheat biomass.

For rapeseed principal phenological stages, the mean kappa index using combined S-1 & 2 data was higher and strongly higher than those obtained with S-2 data alone and S-1 data alone respectively. For secondary phenological stages, results of the combined use of S-1 & 2 data were similar to those obtained with S-2 data alone. However, combined use of S-1 & 2 data increased the accuracy of identifying the leaf development stage of rapeseed thanks to the capture of additional information about physiology from S-2 and geometry from S-1. Development of fruit was the most difficult principal phenological stage to identify using S-1 data alone and the combined use of S-1 & 2 data, due to confusion with ripening (Appendix B, Table B4 and B6 and Fig. 10d and 10f, 11d and 11f). The most important features using S-1 data alone were  $\sigma^{0VH}$ ,  $\sigma^{0VH}:\sigma^{0VV}$  and  $\sigma^{0VV}$ . The temporal profiles showed that the  $\sigma^{0VH}:\sigma^{0VV}$  ratio was stable between development of fruit and ripening, while  $\sigma^{0VH}$  and  $\sigma^{0VV}$  slightly increased. The structure of rapeseed stages is very similar during development of fruit and ripening, with randomly oriented canopy components. This high similarity can be explained by the fact that field observations were conducted during successive phenological stages (i.e. the end of development of fruit (BBCH = 77 and 79) and the beginning and end of ripening (BBCH = 80 and 89)). However, while, the development of fruit was considerably better classified using combined S-1 & 2 data (UA max = 0.87, PA max = 0.75) than using S-1 data alone (UA max = 0.32, PA max = 0.21), this phenological stage was the least well predicted. The most important features using combined S-1 & 2 data were  $\sigma^{0VH}$  derived from S-1 followed by

NDVI and S2REP derived from S-2 and then  $SE_{norm}$ , span,  $SE_i_{norm}$ ,  $\sigma^{0}VH:\sigma^{0}VV$  and  $\sigma^{0}VV$  derived from S-1. Thus, SAR S-1 features increased confusion between development of fruit and ripening stages. The development of fruit was the most difficult secondary phenological stage to identify using S-1 data alone while the beginning and middle of flowering was the least well predicted using S-2 data alone and combined S-1 & 2 data (Fig. 14e and 14f, 15e and 15f). Prediction errors occurred between the two secondary phenological stages of flowering (Appendix C, Tables C5 and C6), the first corresponding to first flowers open until 40% of flowers on main raceme open and the second to the the full flowering until the end of flowering while the petals are fallen. It should be noted that this period coincided to the lack of S-2 data due to cloud cover, while S-1 temporal profiles showed little variation.

Classification results for combined use of S-1 & 2 data pointed out the large contribution of S-1 features for rapeseed. Combined used of S-1 & 2 data identified better principal phenological stages of rapeseed than S-2 data alone; moreover, the identification of the leaf development stage was improved adding S-1 features (Fig. 11c, 11f). Results were more balanced for secondary phenological stages of wheat since S-2 data alone results were similar to those of combined S-1 & 2 data, except for the tillering stage.

## 6. Conclusion

This study evaluated the potential of SAR S-1, optical S-2 time-series and the combined use of S-1 & 2 data to identify principal and secondary phenological stages of wheat and rapeseed. More specifically, we have shown that:

- Combined use of S-1 & 2 data (mean kappa = 0.53-0.82 and 0.74-0.92 for wheat and rapeseed, respectively) was more accurate than using S-1 data alone (mean kappa = 0.48-0.61 and 0.61-0.64 for wheat and rapeseed, respectively) or S-2 data alone (mean kappa = 0.54-0.75 and 0.67-0.86 for wheat and rapeseed, respectively), in identifying principal and secondary phenological stages for both crops.
- S-2 data alone provided better results than S-1 data alone for both crop types.
- Concerning S-1 features, the  $\sigma^{0}VH:\sigma^{0}VV$  ratio and polarimetric indicators were important for obtaining accurate classifications of phenological stages for both crops. These features were the most important for discriminating both crop types using S-1 data alone and combined S-1 & 2 data.
- Concerning S-2 features, LAI, NDVI and S2REP were the most important features for both crop types while the MCARI was less important.
- The number of Sentinel features automatically selected to predict phenological stages of wheat and rapeseed ranged from 4 to 7.

Overall, this study highlighted the value of using polarimetric indicators (Shannon entropy and span) and combining S-1 and 2 data to monitor wheat and rapeseed phenology.

To confirm these results, this method should be based on a larger sample size, especially for identifying secondary phenological stages. Also, to test the robustness of combining S-1 & 2 data to predict principal and secondary phenological stages, the final predictive models should be applied to other study sites.

## Author Contributions

Conceptualization, A.M., L.H-M, Ju.B. (Julie Betbeder) and Ja.B. (Jacques Baudry); Methodology, A.M., Ju.B. and L.H-M.; Software, A.M. and Ju.B.; Validation, A.M.; Resources, Ju.B., V.L.R., F.S. J.L. and D.R.; Data Curation, A.M., V.L.R. and F.S., Writing-Original Draft Preparation, A.M.; Writing-Review & Editing, A.M., L.H-M., Ju.B. and Ja. B; Visualization, A.M., Ju.B. and L.H-M.; Supervision, Ju.B., L.H.-M., and Ja.B.; Project Administration, L.H-M. and Ja.B.; Funding Acquisition, L.H-M. and Ja.B.

## Funding

This research was funded through the 2015-2016 BiodivERsA COFUND call for research proposals, with the national funders ANR, MINECO, and BELSPO, and a Ph.D. grant from the Ministry of Research for A. Mercier.

## Conflicts of Interest

The authors declare no conflict of interest. The funders had no role in the design of the study; in collection, analysis, or interpretation of data; in writing the manuscript; or in the decision to publish the results.

## References

- Álvarez-Mozos, J., Verhoest, N.E.C., Larrañaga, A., Casali, J., González-Audicana, M., 2009. Influence of Surface Roughness Spatial Variability and Temporal Dynamics on the Retrieval of Soil Moisture from SAR Observations. *Sensors* 9, 463–489. <https://doi.org/10.3390/s90100463>
- Ashourloo, D., Shahrabi, H.S., Azadbakht, M., Aghighi, H., Nematollahi, H., Alimohammadi, A., Matkan, A.A., 2019. Automatic canola mapping using time series of sentinel 2 images. *ISPRS Journal of Photogrammetry and Remote Sensing* 156, 63–76. <https://doi.org/10.1016/j.isprsjprs.2019.08.007>
- Baghdadi, N., Boyer, N., Todoroff, P., El Hajj, M., Bégué, A., 2009. Potential of SAR sensors TerraSAR-X, ASAR/ENVISAT and PALSAR/ALOS for monitoring sugarcane crops on Reunion Island. *Remote Sensing of Environment* 113, 1724–1738. <https://doi.org/10.1016/j.rse.2009.04.005>
- Bargiel, D., 2017. A new method for crop classification combining time series of radar images and crop phenology information. *Remote Sens. Environ.* 198, 369–383. <https://doi.org/10.1016/j.rse.2017.06.022>
- Baup, F., Mougin, E., de Rosnay, P., Timouk, F., Chênerie, I., 2007. Surface soil moisture estimation over the AMMA Sahelian site in Mali using ENVISAT/ASAR data. *Remote Sensing of Environment* 109, 473–481. <https://doi.org/10.1016/j.rse.2007.01.015>
- Betbeder, J., Fieuzal, R., Philippets, Y., Ferro-Famil, L., Baup, F., 2016. Contribution of multitemporal polarimetric synthetic aperture radar data for monitoring winter wheat and rapeseed crops. *Journal of Applied Remote Sensing* 10, 026020. <https://doi.org/10.1117/1.JRS.10.026020>
- Bleiholder, H., Weber, E., Hess, M., Wicke, H., van den Boom, T., Lancashire, P.D., Buhr, L., Hack, H., Klose, F.R., Strauss, R., 2001. Growth Stages of Mono- and Dicotyledonous Plants, BBCH Monograph, Federal Biological Research Centre for Agriculture and Forestry: ed. Berlin/Braunschweig, Germany.

- Bontemps, S., Arias, M., Cara, C., Dedieu, G., Guzzonato, E., Hagolle, O., Inglada, J., Matton, N., Morin, D., Popescu, R., Rabaute, T., Savinaud, M., Sepulcre, G., Valero, S., Ahmad, I., Bégué, A., Wu, B., De Abelleira, D., Diarra, A., Dupuy, S., French, A., Ul Hassan Akhtar, I., Kussul, N., Lebourgeois, V., Le Page, M., Newby, T., Savin, I., Verón, S.R., Koetz, B., Defourny, P., 2015. Building a Data Set over 12 Globally Distributed Sites to Support the Development of Agriculture Monitoring Applications with Sentinel-2. *Remote Sensing* 7, 16062–16090. <https://doi.org/10.3390/rs71215815>
- Bouchet, A.-S., Laperche, A., Bissuel-Belaygue, C., Snowdon, R., Nesi, N., Stahl, A., 2016. Nitrogen use efficiency in rapeseed. A review. *Agron. Sustain. Dev.* 36, 38. <https://doi.org/10.1007/s13593-016-0371-0>
- Bouman, B.A.M., van Kasteren, H.W.J., Uenk, D., 1992. Standard relations to estimate ground cover and LAI of agricultural crops from reflectance measurements. *European Journal of Agronomy* 1, 249–262. [https://doi.org/10.1016/S1161-0301\(14\)80077-4](https://doi.org/10.1016/S1161-0301(14)80077-4)
- Brown, S.C.M., Quegan, S., Morrison, K., Bennett, J.C., Cookmartin, G., 2003. High-resolution measurements of scattering in wheat canopies-implications for crop parameter retrieval. *IEEE Transactions on Geoscience and Remote Sensing* 41, 1602–1610. <https://doi.org/10.1109/TGRS.2003.814132>
- Calle, M.L., Urrea, V., 2011. Letter to the Editor: Stability of Random Forest importance measures. *Brief Bioinform* 12, 86–89. <https://doi.org/10.1093/bib/bbq011>
- Canisius, F., Shang, J., Liu, J., Huang, X., Ma, B., Jiao, X., Geng, X., Kovacs, J.M., Walters, D., 2018. Tracking crop phenological development using multi-temporal polarimetric Radarsat-2 data. *Remote Sensing of Environment* 210, 508–518. <https://doi.org/10.1016/j.rse.2017.07.031>
- Clevers, J.G.P.W., 1988. The derivation of a simplified reflectance model for the estimation of leaf area index. *Remote Sensing of Environment* 25, 53–69. [https://doi.org/10.1016/0034-4257\(88\)90041-7](https://doi.org/10.1016/0034-4257(88)90041-7)
- Clevers, J.G.P.W., Gitelson, A.A., 2013. Remote estimation of crop and grass chlorophyll and nitrogen content using red-edge bands on Sentinel-2 and -3. *International Journal of Applied Earth Observation and Geoinformation* 23, 344–351. <https://doi.org/10.1016/j.jag.2012.10.008>
- Clevers, J.G.P.W., Jong, S.M.D., Epema, G.F., Meer, F.D.V.D., Bakker, W.H., Skidmore, A.K., Scholte, K.H., 2002. Derivation of the red edge index using the MERIS standard band setting. *International Journal of Remote Sensing* 23, 3169–3184. <https://doi.org/10.1080/01431160110104647>
- Clevers, J.G.P.W., Kooistra, L., Van den Brande, M.M.M., 2017. Using Sentinel-2 Data for Retrieving LAI and Leaf and Canopy Chlorophyll Content of a Potato Crop. *Remote Sensing* 9, 405. <https://doi.org/10.3390/rs9050405>
- Cohen, J., 1960. A Coefficient of Agreement for Nominal Scales. *Educational and Psychological Measurement* 20, 37–46. <https://doi.org/10.1177/001316446002000104>
- Congalton, R.G., 1991. A review of assessing the accuracy of classifications of remotely sensed data. *Remote Sensing of Environment* 37, 35–46. [https://doi.org/10.1016/0034-4257\(91\)90048-B](https://doi.org/10.1016/0034-4257(91)90048-B)
- Cookmartin, G., Saich, P., Quegan, S., Cordey, R., Burgess-Allen, P., Sowter, A., 2000. Modeling microwave interactions with crops and comparison with ERS-2 SAR observations. *IEEE Transactions on Geoscience and Remote Sensing* 38, 658–670. <https://doi.org/10.1109/36.841996>

Daughtry, C.S.T., Walthall, C.L., Kim, M.S., de Colstoun, E.B., McMurtrey, J.E., 2000. Estimating Corn Leaf Chlorophyll Concentration from Leaf and Canopy Reflectance. *Remote Sensing of Environment* 74, 229–239. [https://doi.org/10.1016/S0034-4257\(00\)00113-9](https://doi.org/10.1016/S0034-4257(00)00113-9)

Delegido, J., Verrelst, J., Alonso, L., Moreno, J., 2011. Evaluation of Sentinel-2 Red-Edge Bands for Empirical Estimation of Green LAI and Chlorophyll Content. *Sensors* 11, 7063–7081. <https://doi.org/10.3390/s110707063>

Dente, L., Satalino, G., Mattia, F., Rinaldi, M., 2008. Assimilation of leaf area index derived from ASAR and MERIS data into CERES-Wheat model to map wheat yield. *Remote Sensing of Environment, Remote Sensing Data Assimilation Special Issue* 112, 1395–1407. <https://doi.org/10.1016/j.rse.2007.05.023>

Diacono, M., Rubino, P., Montemurro, F., 2013. Precision nitrogen management of wheat. A review. *Agronomy for Sustainable Development* 33, 219–241. <https://doi.org/10.1007/s13593-012-0111-z>

Doraiswamy, P.C., Hatfield, J.L., Jackson, T.J., Akhmedov, B., Prueger, J., Stern, A., 2004. Crop condition and yield simulations using Landsat and MODIS. *Remote Sensing of Environment* 92, 548–559. <https://doi.org/10.1016/j.rse.2004.05.017>

Duchemin, B., Fieuzal, R., Rivera, M.A., Ezzahar, J., Jarlan, L., Rodriguez, J.C., Hagolle, O., Watts, C., 2015. Impact of Sowing Date on Yield and Water Use Efficiency of Wheat Analyzed through Spatial Modeling and FORMOSAT-2 Images. *Remote Sensing* 7, 5951–5979. <https://doi.org/10.3390/rs70505951>

El Hajj, M., Baghdadi, N., Bazzi, H., Zribi, M., 2019. Penetration Analysis of SAR Signals in the C and L Bands for Wheat, Maize, and Grasslands. *Remote Sensing* 11, 31. <https://doi.org/10.3390/rs11010031>

Ferro-Famil, L., Pottier, E., 2014. Chapter 21 - Radar Polarimetry Basics and Selected Earth Remote Sensing Applications, in: Sidiropoulos, N.D., Gini, F., Chellappa, R., Theodoridis, S. (Eds.), *Academic Press Library in Signal Processing*. Elsevier, pp. 1119–1244. <https://doi.org/10.1016/B978-0-12-396500-4.00021-1>

Fieuzal, R., Baup, F., Marais-Sicre, C., 2013. Monitoring Wheat and Rapeseed by Using Synchronous Optical and Radar Satellite Data—From Temporal Signatures to Crop Parameters Estimation. *Advances in Remote Sensing* 02, 162–180. <https://doi.org/10.4236/ars.2013.22020>

Food and Agriculture Organization of the United Nations, 2017. FAOSTAT [WWW Document]. F. Statistical databases. URL <http://www.fao.org/faostat/en/#data/QC> (accessed 5.17.19).

Frampton, W.J., Dash, J., Watmough, G., Milton, E.J., 2013. Evaluating the capabilities of Sentinel-2 for quantitative estimation of biophysical variables in vegetation. *ISPRS Journal of Photogrammetry and Remote Sensing* 82, 83–92. <https://doi.org/10.1016/j.isprsjprs.2013.04.007>

Gao, S., Niu, Z., Huang, N., Hou, X., 2013. Estimating the Leaf Area Index, height and biomass of maize using HJ-1 and RADARSAT-2. *International Journal of Applied Earth Observation and Geoinformation* 24, 1–8. <https://doi.org/10.1016/j.jag.2013.02.002>

Guyot, G., Baret, F., 1988. Utilisation de la haute resolution spectrale pour suivre l'état des couverts vegetaux. *Spectral Signatures of Objects in Remote Sensing* 287, 279.

Haboudane, D., Miller, J.R., Pattey, E., Zarco-Tejada, P.J., Strachan, I.B., 2004. Hyperspectral vegetation indices and novel algorithms for predicting green LAI of crop canopies: Modeling and validation in the context of precision agriculture. *Remote Sensing of Environment* 90, 337–352. <https://doi.org/10.1016/j.rse.2003.12.013>

Hatfield, J.L., Gitelson, A.A., Schepers, J.S., Walthall, C.L., 2008. Application of Spectral Remote Sensing for Agronomic Decisions. *Agronomy Journal* 100, S-117. <https://doi.org/10.2134/agronj2006.0370c>

- Hatfield, J.L., Prueger, J.H., Sauer, T.J., Dold, C., O'Brien, P., Wacha, K., 2019. Applications of Vegetative Indices from Remote Sensing to Agriculture: Past and Future. *Inventions* 4, 71. <https://doi.org/10.3390/inventions4040071>
- Hatfield, P.L., Pinter, P.J., 1993. Remote sensing for crop protection. *Crop Protection* 12, 403–413. [https://doi.org/10.1016/0261-2194\(93\)90001-Y](https://doi.org/10.1016/0261-2194(93)90001-Y)
- Herrmann, I., Pimstein, A., Karnieli, A., Cohen, Y., Alchanatis, V., Bonfil, D.J., 2011. LAI assessment of wheat and potato crops by VEN $\mu$ S and Sentinel-2 bands. *Remote Sensing of Environment* 115, 2141–2151. <https://doi.org/10.1016/j.rse.2011.04.018>
- Homayouni, S., McNairn, H., Hosseini, M., Jiao, X., Powers, J., 2019. Quad and compact multitemporal C-band PolSAR observations for crop characterization and monitoring. *International Journal of Applied Earth Observation and Geoinformation* 74, 78–87. <https://doi.org/10.1016/j.jag.2018.09.009>
- Inglada, J., Vincent, A., Arias, M., Marais-Sicre, C., 2016. Improved Early Crop Type Identification By Joint Use of High Temporal Resolution SAR And Optical Image Time Series. *Remote Sens.* 8, 362. <https://doi.org/10.3390/rs8050362>
- Jamoneau, A., 2010. Relations entre les diversités alpha, bêta et gamma de la flore vasculaire de fragments forestiers inclus dans des paysages agricoles contrastés (Doctoral dissertation). Université de Picardie Jules Verne.
- Jiao, X., McNairn, H., Shang, J., Pattey, E., Liu, J., Champagne, C., 2009. The sensitivity of RADARSAT-2 quad-polarization SAR data to crop LAI, in: *Remote Sensing and Modeling of Ecosystems for Sustainability VI*. Presented at the Remote Sensing and Modeling of Ecosystems for Sustainability VI, International Society for Optics and Photonics, p. 745400. <https://doi.org/10.1117/12.825701>
- Jin, X., Kumar, L., Li, Z., Feng, H., Xu, X., Yang, G., Wang, J., 2018. A review of data assimilation of remote sensing and crop models. *European Journal of Agronomy* 92, 141–152. <https://doi.org/10.1016/j.eja.2017.11.002>
- Jin, X., Yang, G., Xu, X., Yang, H., Feng, H., Li, Z., Shen, J., Lan, Y., Zhao, C., 2015. Combined Multi-Temporal Optical and Radar Parameters for Estimating LAI and Biomass in Winter Wheat Using HJ and RADARSAR-2 Data. *Remote Sensing* 7, 13251–13272. <https://doi.org/10.3390/rs71013251>
- Khoshgoftaar, T.M., Golawala, M., Hulse, J.V., 2007. An Empirical Study of Learning from Imbalanced Data Using Random Forest, in: *19th IEEE International Conference on Tools with Artificial Intelligence (ICTAI 2007)*. Presented at the 19th IEEE International Conference on Tools with Artificial Intelligence (ICTAI 2007), pp. 310–317. <https://doi.org/10.1109/ICTAI.2007.46>
- Lee, J.S., Jurkevich, L., Dewaele, P., Wambacq, P., Oosterlinck, A., 1994. Speckle filtering of synthetic aperture radar images: A review. *Remote Sensing Reviews* 8, 255–267. <https://doi.org/10.1080/02757259409532206>
- Lopez-Sanchez, J.M., Vicente-Guijalba, F., Ballester-Berman, J.D., Cloude, S.R., 2013. Estimating Phenology Of Agricultural Crops From Space. Presented at the ESA Living Planet Symposium, p. 115.
- Maas, S.J., 1988. Use of remotely-sensed information in agricultural crop growth models. *Ecological Modelling* 41, 247–268. [https://doi.org/10.1016/0304-3800\(88\)90031-2](https://doi.org/10.1016/0304-3800(88)90031-2)

- Mandal, D., Kumar, V., Bhattacharya, A., Rao, Y.S., Siqueira, P., Bera, S., 2018. Sen4Rice: A Processing Chain for Differentiating Early and Late Transplanted Rice Using Time-Series Sentinel-1 SAR Data With Google Earth Engine. *IEEE Trans. Geosci. Remote Sens. Lett.* 1–5. <https://doi.org/10.1109/LGRS.2018.2865816>
- McNairn, H., Brisco, B., 2004. The application of C-band polarimetric SAR for agriculture: a review. *Can. J. Remote Sensing* 30, 525–542. <https://doi.org/10.5589/m03-069>
- McNairn, H., Jiao, X., Pacheco, A., Sinha, A., Tan, W., Li, Y., 2018. Estimating canola phenology using synthetic aperture radar. *Remote Sensing of Environment* 219, 196–205. <https://doi.org/10.1016/j.rse.2018.10.012>
- Menzel, A., Sparks, T.H., Estrella, N., Koch, E., Aasa, A., Ahas, R., Alm-Kübler, K., Bissolli, P., Braslavská, O., Briede, A., Chmielewski, F.M., Crepinsek, Z., Curnel, Y., Dahl, Å., Defila, C., Donnelly, A., Filella, Y., Jatczak, K., Måge, F., Mestre, A., Nordli, Ø., Peñuelas, J., Pirinen, P., Remišová, V., Scheifinger, H., Striz, M., Susnik, A., Vliet, A.J.H.V., Wielgolaski, F.-E., Zach, S., Zust, A., 2006. European phenological response to climate change matches the warming pattern. *Global Change Biology* 12, 1969–1976. <https://doi.org/10.1111/j.1365-2486.2006.01193.x>
- Mercier, A., Betbeder, J., Rumiano, F., Baudry, J., Gond, V., Blanc, L., Bourgoïn, C., Cornu, G., Ciudad, C., Marchamalo, M., Pocard-Chapuis, R., Hubert-Moy, L., 2019. Evaluation of Sentinel-1 and 2 Time Series for Land Cover Classification of Forest–Agriculture Mosaics in Temperate and Tropical Landscapes. *Remote Sensing* 11, 979. <https://doi.org/10.3390/rs11080979>
- Miranda, N., Meadows, P.J., 2015. Radiometric Calibration of S-1 Level-1 Products Generated by the S-1 ipf. Viewed at <https://sentinel.esa.int/documents/247904/685163/S1-Radiometric-Calibration-V1.0.pdf>.
- Mulla, D.J., 2013. Twenty five years of remote sensing in precision agriculture: Key advances and remaining knowledge gaps. *Biosystems Engineering, Special Issue: Sensing Technologies for Sustainable Agriculture* 114, 358–371. <https://doi.org/10.1016/j.biosystemseng.2012.08.009>
- Pacheco, A., McNairn, H., Li, Y., Lampropoulos, G., Powers, J., 2016. Using RADARSAT-2 and TerraSAR-X satellite data for the identification of canola crop phenology, in: *Remote Sensing for Agriculture, Ecosystems, and Hydrology XVIII*. Presented at the Remote Sensing for Agriculture, Ecosystems, and Hydrology XVIII, International Society for Optics and Photonics, p. 999802. <https://doi.org/10.1117/12.2240789>
- Pan, H., Chen, Z., Ren, J., Li, H., Wu, S., 2018. Modeling Winter Wheat Leaf Area Index and Canopy Water Content With Three Different Approaches Using Sentinel-2 Multispectral Instrument Data. *IEEE Journal of Selected Topics in Applied Earth Observations and Remote Sensing* 1–11. <https://doi.org/10.1109/JSTARS.2018.2855564>
- Pan, Z., Huang, J., Zhou, Q., Wang, L., Cheng, Y., Zhang, H., Blackburn, G.A., Yan, J., Liu, J., 2015. Mapping crop phenology using NDVI time-series derived from HJ-1 A/B data. *International Journal of Applied Earth Observation and Geoinformation* 34, 188–197. <https://doi.org/10.1016/j.jag.2014.08.011>
- Pelletier, C., Valero, S., Inglada, J., Champion, N., Dedieu, G., 2016. Assessing the robustness of Random Forests to map land cover with high resolution satellite image time series over large areas. *Remote Sensing of Environment* 187, 156–168. <https://doi.org/10.1016/j.rse.2016.10.010>
- Pottier, E., Ferro-Famil, L., 2012. PolSARPro V5.0: An ESA educational toolbox used for self-education in the field of POLSAR and POL-INSAR data analysis, in: *2012 IEEE International Geoscience and Remote*



Sensing Symposium. Presented at the 2012 IEEE International Geoscience and Remote Sensing Symposium, pp. 7377–7380. <https://doi.org/10.1109/IGARSS.2012.6351925>

Quarmby, N.A., Milnes, M., Hindle, T.L., Silleos, N., 1993. The use of multi-temporal NDVI measurements from AVHRR data for crop yield estimation and prediction. *International Journal of Remote Sensing* 14, 199–210. <https://doi.org/10.1080/01431169308904332>

Rosenfield, G.H., Fitzpatrick-Lins, K., 1986. A coefficient of agreement as a measure of thematic classification accuracy. *Photogrammetric Engineering and Remote Sensing* 52, 5.

Rouse, J.W.J., Haas, R.H., Schell, J.A., Deering, D.W., 1973. Monitoring vegetation systems in the Great Plains with ERTS. Presented at the Third ERTS-1 Symposium, NASA, Washington, DC, USA.

Sakamoto, T., Yokozawa, M., Toritani, H., Shibayama, M., Ishitsuka, N., Ohno, H., 2005. A crop phenology detection method using time-series MODIS data. *Remote Sensing of Environment* 96, 366–374. <https://doi.org/10.1016/j.rse.2005.03.008>

Song, Y., Wang, J., 2019. Mapping Winter Wheat Planting Area and Monitoring Its Phenology Using Sentinel-1 Backscatter Time Series. *Remote Sensing* 11, 449. <https://doi.org/10.3390/rs11040449>

Steele-Dunne, S.C., McNairn, H., Monsivais-Huertero, A., Judge, J., Liu, P., Papathanassiou, K., 2017. Radar Remote Sensing of Agricultural Canopies: A Review. *IEEE Journal of Selected Topics in Applied Earth Observations and Remote Sensing* 10, 2249–2273. <https://doi.org/10.1109/JSTARS.2016.2639043>

Stendardi, L., Karlsen, S.R., Niedrist, G., Gerdol, R., Zebisch, M., Rossi, M., Notarnicola, C., 2019. Exploiting Time Series of Sentinel-1 and Sentinel-2 Imagery to Detect Meadow Phenology in Mountain Regions. *Remote Sensing* 11, 542. <https://doi.org/10.3390/rs11050542>

Veloso, A., Mermoz, S., Bouvet, A., Le Toan, T., Planells, M., Dejoux, J.-F., Ceschia, E., 2017. Understanding the temporal behavior of crops using Sentinel-1 and Sentinel-2-like data for agricultural applications. *Remote Sensing of Environment* 199, 415–426. <https://doi.org/10.1016/j.rse.2017.07.015>

Vreugdenhil, M., Wagner, W., Bauer-Marschallinger, B., Pfeil, I., Teubner, I., Rüdiger, C., Strauss, P., 2018. Sensitivity of Sentinel-1 Backscatter to Vegetation Dynamics: An Austrian Case Study. *Remote Sensing* 10, 1396. <https://doi.org/10.3390/rs10091396>

Wilson, J., Zhang, C., Kovacs, J., 2014. Separating Crop Species in Northeastern Ontario Using Hyperspectral Data. *Remote Sensing* 6, 925–945. <https://doi.org/10.3390/rs6020925>

Wiseman, G., McNairn, H., Homayouni, S., Shang, J., 2014. RADARSAT-2 Polarimetric SAR Response to Crop Biomass for Agricultural Production Monitoring. *IEEE Journal of Selected Topics in Applied Earth Observations and Remote Sensing* 7, 4461–4471. <https://doi.org/10.1109/JSTARS.2014.2322311>

## Appendix A

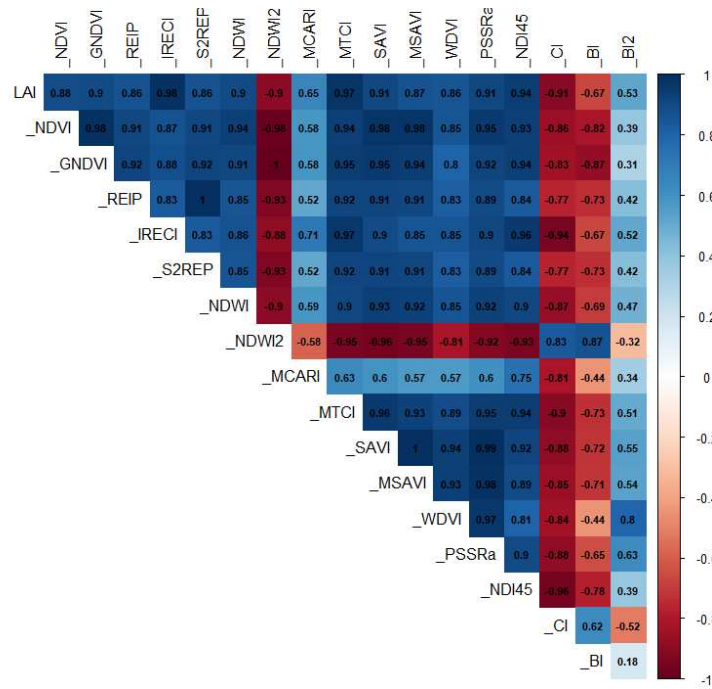


Figure A1. Correlation matrix of features derived from S-2 images for wheat

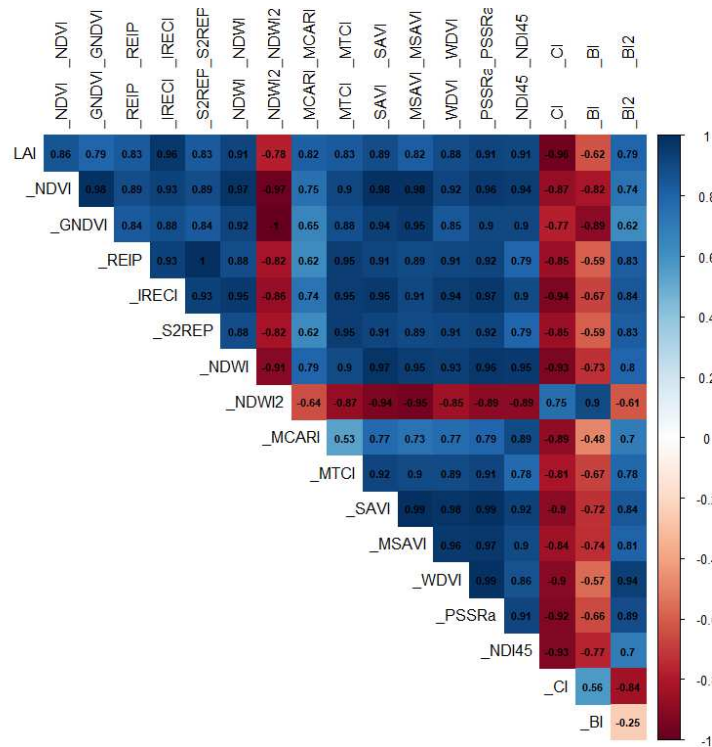


Figure A2. Correlation matrix of features derived from S-2 images for rapeseed

## Appendix B

**Table B1.** Confusion matrix of the principal phenological stages of wheat classification derived from the 4 most important features of S-1 data alone (lines) and the validation (columns). The classification was performed using the first pair of randomly generated training and validation samples.

Classification	Code	Validation					Total
		1	2	3	4	5	
Tillering	1	13				1	14
Stem elongation	2		9	1	2		12
Flowering	3		2	1	2	1	6
Development of fruit	4		1	5	8	2	18
Ripening	5					7	
<b>Total</b>		<b>14</b>	<b>13</b>	<b>8</b>	<b>14</b>	<b>11</b>	
<b>Kappa index</b>		<b>0.54</b>					
<b>Overall Accuracy</b>		<b>63%</b>					

**Table B2.** Confusion matrix of the principal phenological stages of wheat classification derived from the 8 most important features of S-2 data alone (lines) and the validation (columns). The classification was performed using the first pair of randomly generated training and validation samples.

Classification	Code	Validation					Total
		1	2	3	4	5	
Tillering	1	13					13
Stem elongation	2		11		1		12
Flowering	3			6	1		7
Development of fruit	4		2	2	12	4	20
Ripening	5	1				7	8
<b>Total</b>		<b>14</b>	<b>13</b>	<b>8</b>	<b>14</b>	<b>11</b>	
<b>Kappa index</b>		<b>0.77</b>					
<b>Overall Accuracy</b>		<b>82%</b>					

**Table B3.** Confusion matrix of the principal phenological stages of wheat classification derived from the 9 most important features of combined S-1 & 2 data (lines) and the validation (columns). The classification was performed using the first pair of randomly generated training and validation samples.

Classification	Code	Validation					Total
		1	2	3	4	5	
Tillering	1	13				1	14
Stem elongation	2		8		2		10
Flowering	3			6			6
Development of fruit	4		4	2	12	1	19
Ripening	5	1	1			9	11
<b>Total</b>		<b>14</b>	<b>13</b>	<b>8</b>	<b>14</b>	<b>11</b>	
<b>Kappa index</b>		<b>0.75</b>					
<b>Overall Accuracy</b>		<b>80%</b>					

**Table B4.** Confusion matrix of the principal phenological stages of rapeseed classification derived from the 4 most important features of S-1 data alone (lines) and the validation (columns). The classification was performed using the first pair of randomly generated training and validation samples.

Classification	Code	Validation					Total
		1	2	3	4	5	
Leaf development	1	4		2			6
Inflorescence emergence	2		11	1		1	13
Flowering	3	2		9			11
Development of fruit	4				1	1	2
Ripening	5		1		4	8	12
<b>Total</b>		<b>6</b>	<b>12</b>	<b>12</b>	<b>5</b>	<b>10</b>	
<b>Kappa index</b>		<b>0.65</b>					
<b>Overall Accuracy</b>		<b>73%</b>					

**Table B5.** Confusion matrix of the principal phenological stages of rapeseed classification derived from the 6 most important features of S-2 data alone (lines) and the validation (columns). The classification was performed using the first pair of randomly generated training and validation samples.

Classification	Code	Validation					Total
		1	2	3	4	5	
Leaf development	1	5					5
Inflorescence emergence	2		11	1		2	13
Flowering	3			11			11
Development of fruit	4				4		4
Ripening	5	1	1		1	8	11
<b>Total</b>		<b>6</b>	<b>12</b>	<b>12</b>	<b>5</b>	<b>10</b>	
<b>Kappa index</b>		<b>0.83</b>					
<b>Overall Accuracy</b>		<b>87%</b>					

**Table B6.** Confusion matrix of the principal phenological stages of rapeseed classification derived from the 10 most important features of combined S-1 & 2 data (lines) and the validation (columns). The classification was performed using the first pair of randomly generated training and validation samples.

Classification	Code	Validation					Total
		1	2	3	4	5	
Leaf development	1	6		1			7
Inflorescence emergence	2		12				12
Flowering	3			11			11
Development of fruit	4				4		4
Ripening	5				1	10	11
<b>Total</b>		<b>6</b>	<b>12</b>	<b>12</b>	<b>5</b>	<b>10</b>	
<b>Kappa index</b>		<b>96%</b>					
<b>Overall Accuracy</b>		<b>0.94</b>					

## Appendix C

**Table C1.** Confusion matrix of the secondary phenological stages of wheat classification derived from the 4 most important features of S-1 data alone (lines) and the validation (columns). The classification was performed using the first pair of randomly generated training and validation samples.

Classification	Code	Validation							Total
		1	2	3	4	5	6	7	
Beginning of tillering	1	11	2				1		14
Middle/end of tillering	2	2	16						18
Stem elongation	3			9		2			11
Flowering, anthesis	4			2	1	2	2		7
Development of fruit	5			2	6	9	2	1	20
Middle of ripening	6					1	1		2
End of ripening	7				1		3	1	5
Total		13	18	13	8	14	9	2	
Kappa index	0.55								
Overall Accuracy	62%								

**Table C2.** Confusion matrix of the secondary phenological stages of wheat classification derived from the 5 most important features of S-2 data alone (lines) and the validation (columns). The classification was performed using the first pair of randomly generated training and validation samples.

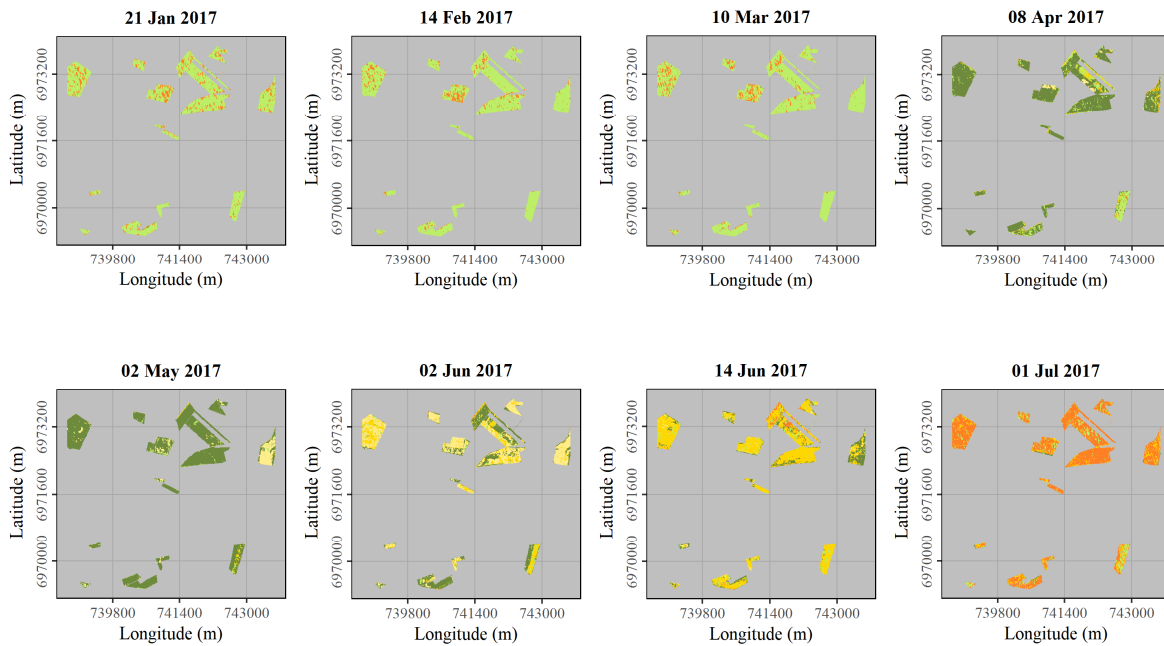
Classification	Code	Validation							Total
		1	2	3	4	5	6	7	
Beginning of tillering	1	11	2						13
Middle/end of tillering	2	1	16				1		17
Stem elongation	3			12					12
Flowering, anthesis	4				6	1			7
Development of fruit	5			1	2	12	4		19
Middle of ripening	6					1	2		3
End of ripening	7	1					2	2	5
Total		13	18	13	8	14	9	2	
Kappa index	0.75								
Overall Accuracy	79%								

**Table C3.** Confusion matrix of the secondary phenological stages of wheat classification derived from the 9 most important features of combined S-1 & 2 data (lines) and the validation (columns). The classification was performed using the first pair of randomly generated training and validation samples.

Classification	Code	Validation							Total
		1	2	3	4	5	6	7	
Beginning of tillering	1	12	1						13
Middle/end of tillering	2	1	17				1		18
Stem elongation	3			9	1	2			12
Flowering, anthesis	4				5				5
Development of fruit	5			3	2	12	1		18
Middle of ripening	6			1			4		5
End of ripening	7						3	2	5
Total		13	18	13	8	14	9	2	
Kappa index	0.75								
Overall Accuracy	79%								

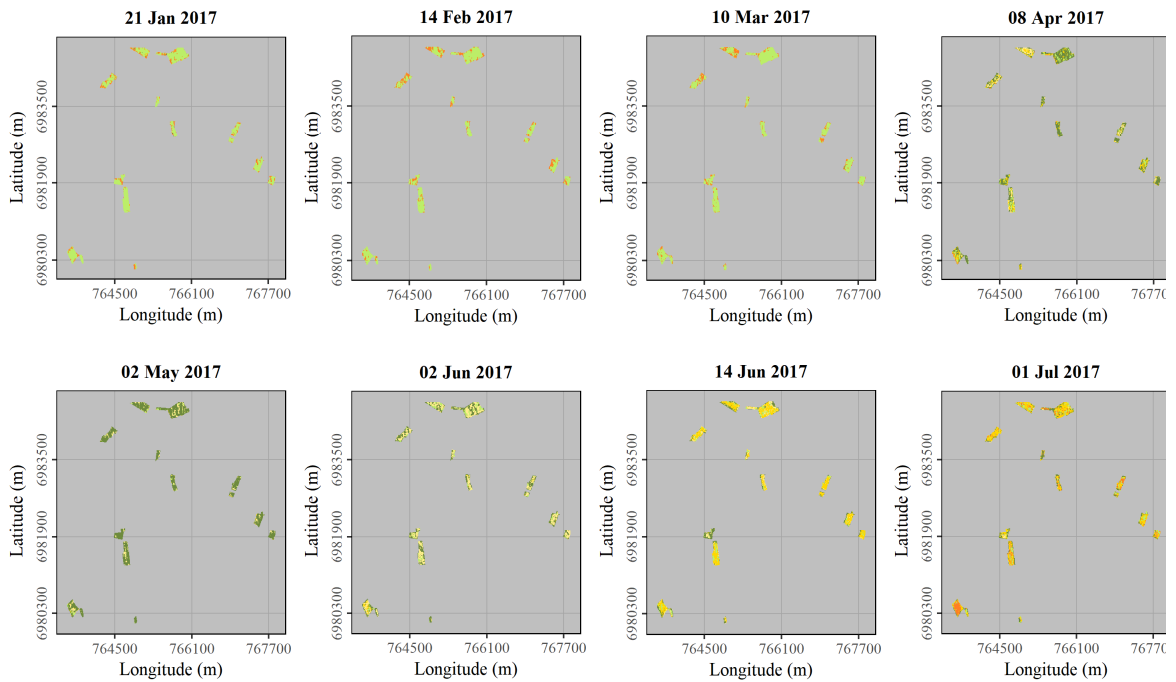


## Appendix D



■ Tilling    
 ■ Stem elongation    
 ■ Flowering, anthesis    
 ■ Dev. of fruit    
 ■ Ripenin

**Figure D1.** Classification of the 5 principal phenological stages of wheat in the open field study site using combined Sentinel-1 & 2 data.



■ Tilling    
 ■ Stem elongation    
 ■ Flowering, anthesis    
 ■ Dev. of fruit    
 ■ Ripenin

**Figure D2.** Classification of the 5 principal phenological stages of wheat in the bocage study site using combined Sentinel-1 & 2 data.

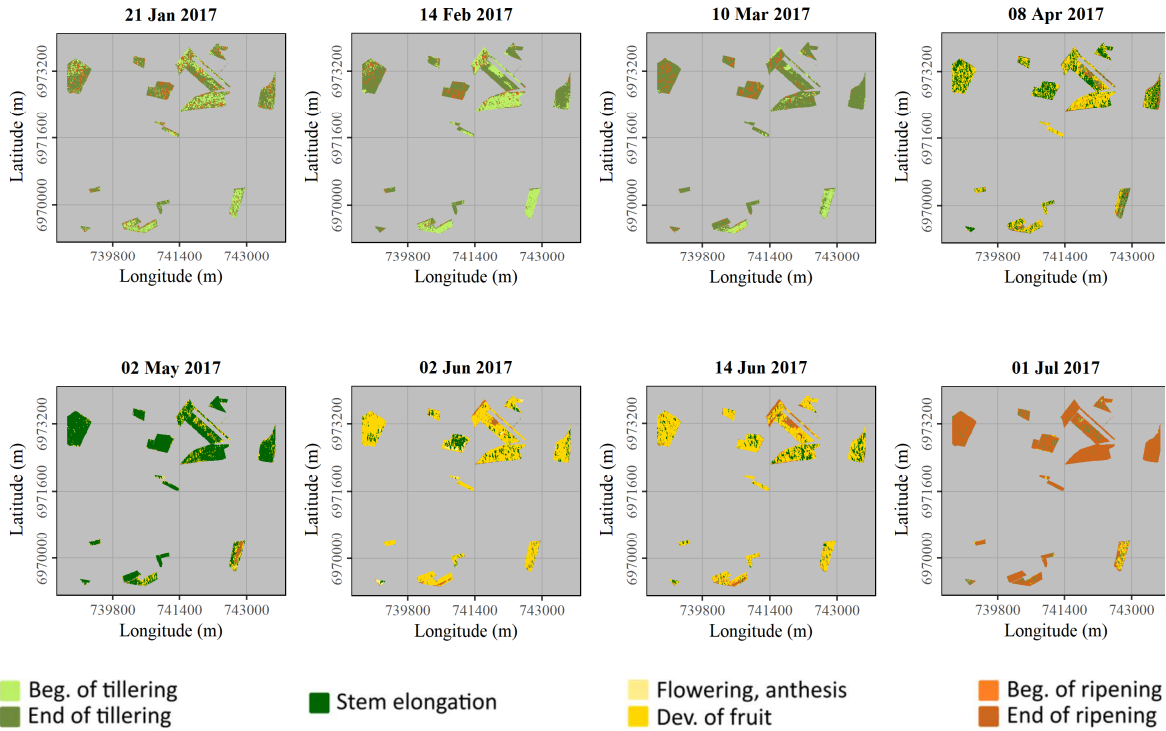


**Figure D3.** Classification of the 7 secondary phenological stages of wheat in the open field study site using combined Sentinel-1 & 2 data.

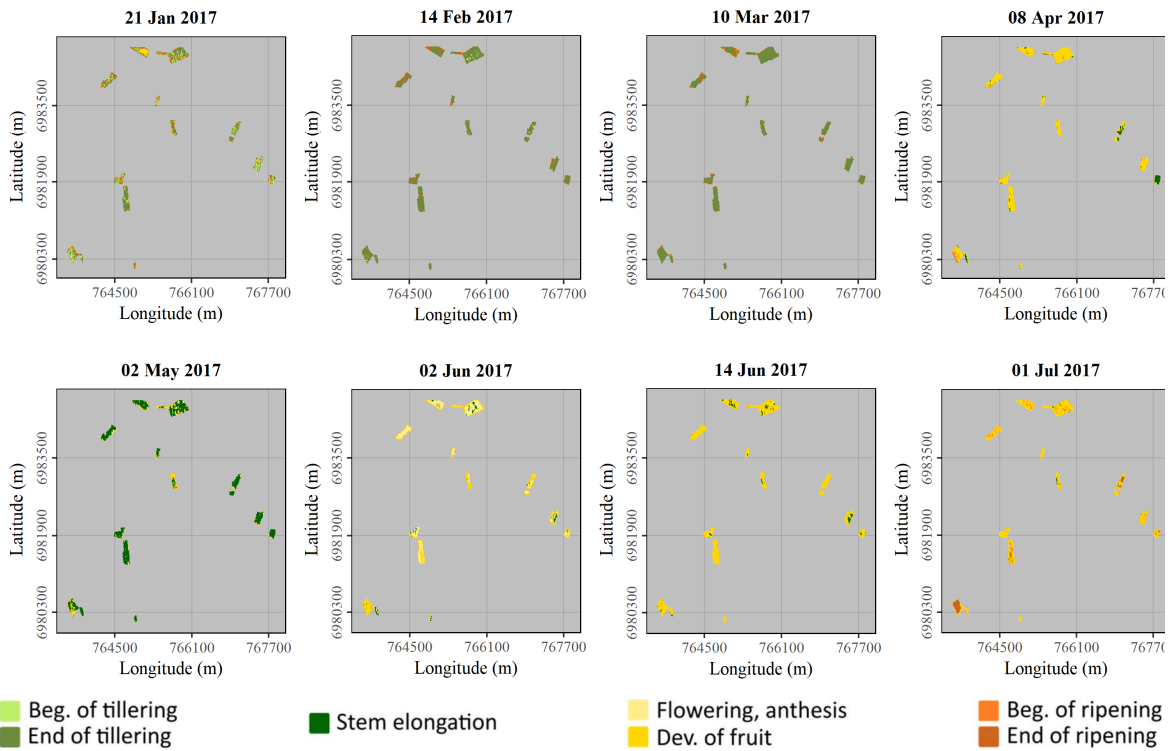


**Figure D4.** Classification of the 7 secondary phenological stages of wheat in the bogage study site using combined Sentinel-1 & 2 data.



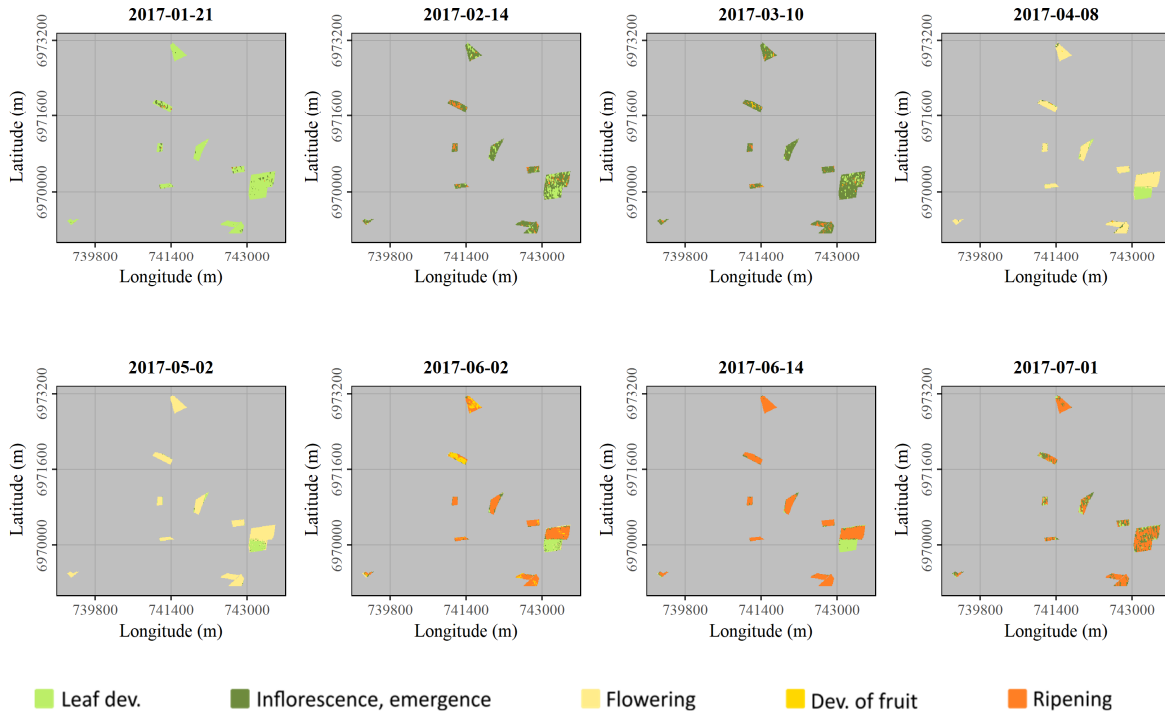


**Figure D5.** Classification of the 5 principal phenological stages of rapeseed in the open field study site using combined Sentinel-1 & 2 data.

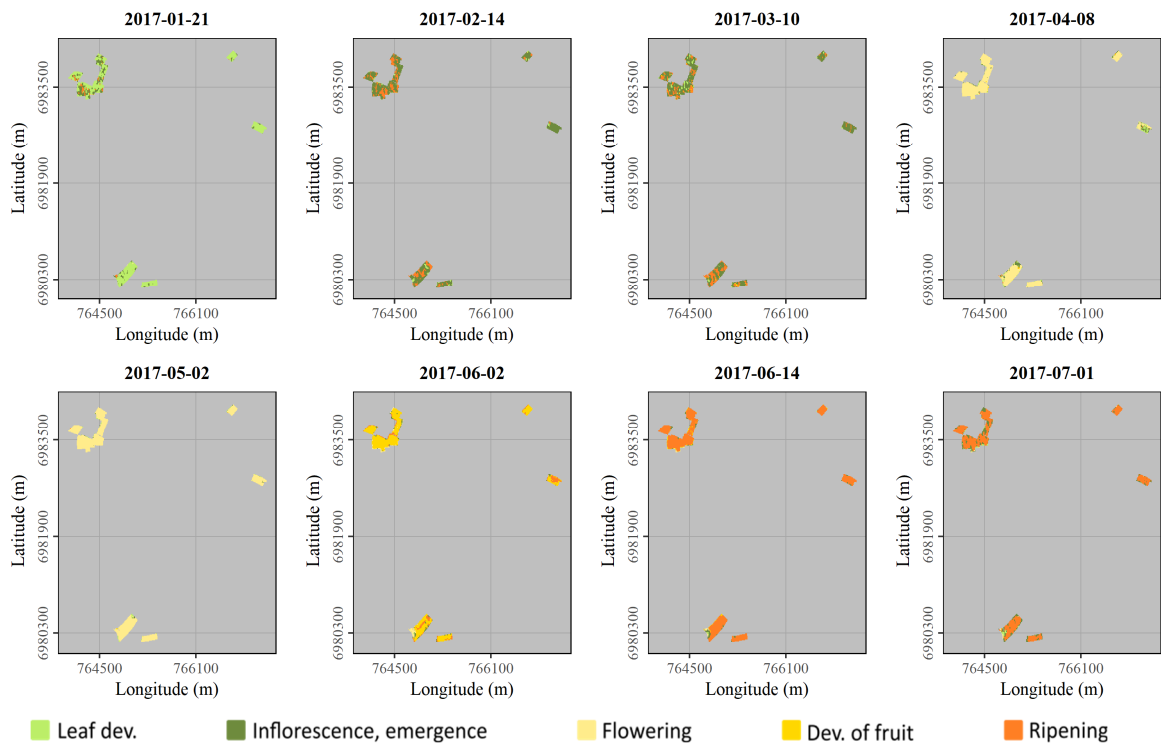
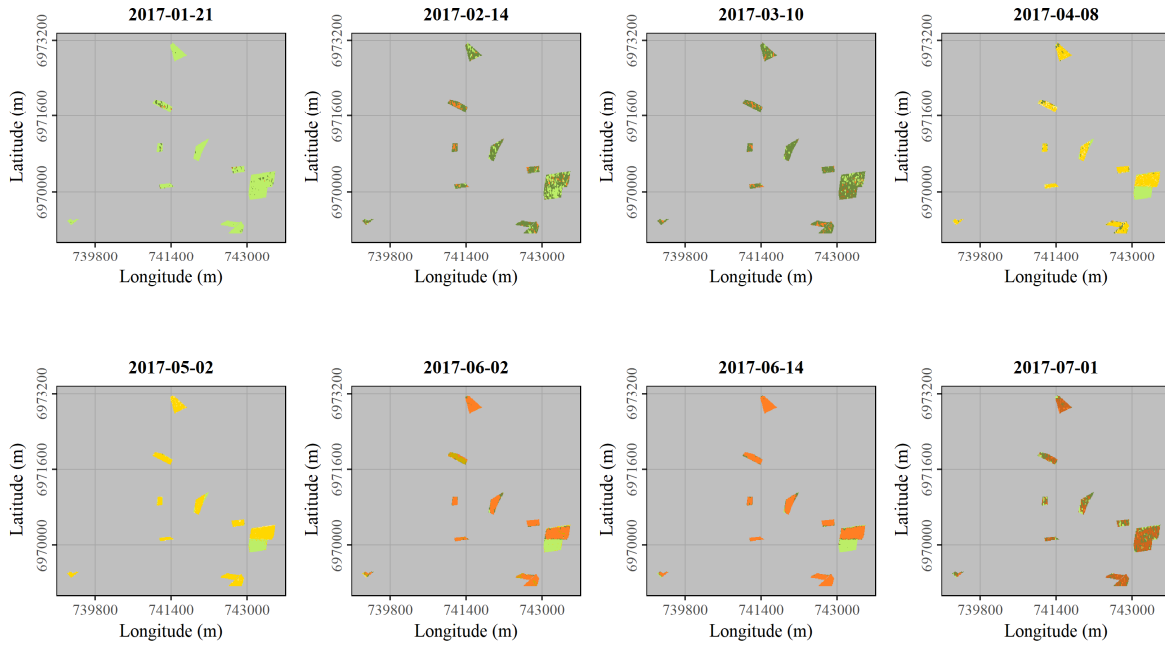
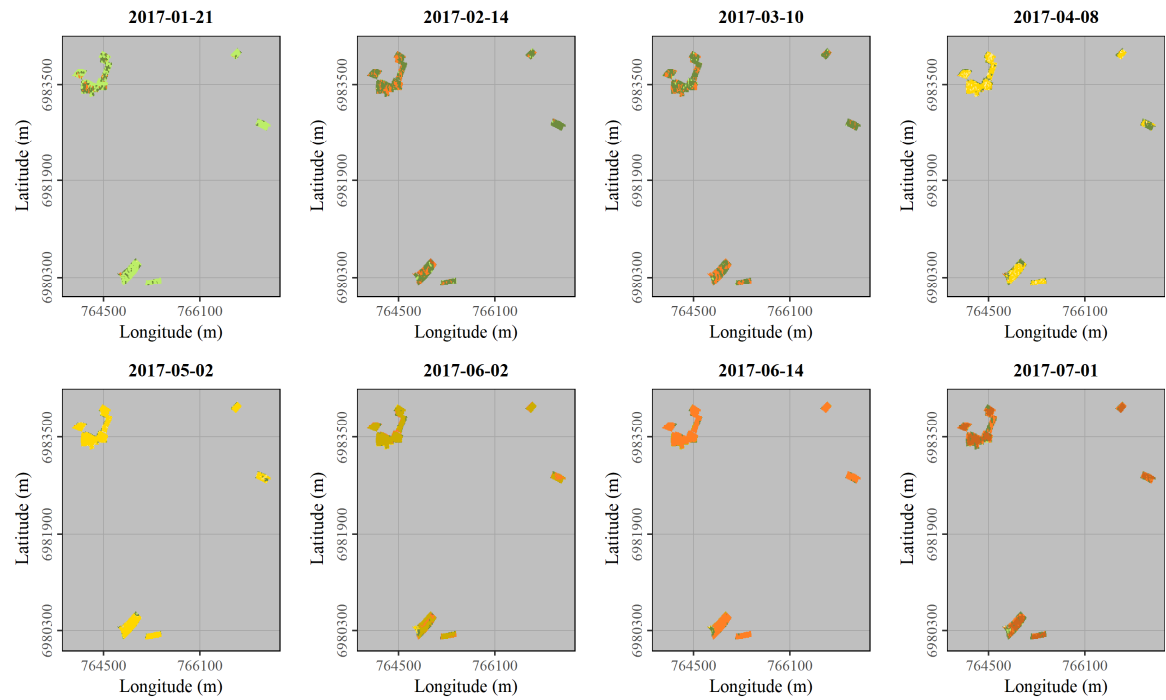


**Figure D6.** Classification of the 5 principal phenological stages of rapeseed in the bogage study site using combined Sentinel-1 & 2 data.



- Leaf dev.
- Inflorescence, emergence
- Beg./middle of flowering
- End of flowering
- Dev. of fruit
- Beg. of ripening
- End of ripening

**Figure D7.** Classification of the 7 secondary phenological stages of rapeseed in the open field study site using combined Sentinel-1 & 2 data.



- Leaf dev.
- Inflorescence, emergence
- Beg./middle of flowering
- End of flowering
- Dev. of fruit
- Beg. of ripening
- End of ripening

**Figure D8.** Classification of the 7 secondary phenological stages of rapeseed in the bocage study site using combined Sentinel-1 & 2 data.